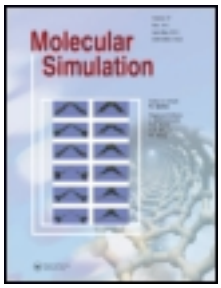

Molecular Simulation
Publication details, including instructions for authors and subscription information:
http://www.tandfonline.com/loi/gmos20

Interfacial water on crystalline silica: a comparative molecular dynamics simulation study

Tuan A. Ho [a], Dimitrios Argyris [a], Dimitrios V. Papavassiliou [a], Alberto Striolo [a], Lloyd L. Lee [b] & David R. Cole [c]

[a] School of Chemical, Biological, and Materials Engineering, The University of Oklahoma, Norman, OK, 73019, USA

[b] Department of Chemical and Materials Engineering, California State Polytechnic University, Pomona, CA, 91768, USA

[c] School of Earth Sciences, The Ohio State University, Columbus, OH, 43210, USA

Available online: 03 Mar 2011

To cite this article: Tuan A. Ho, Dimitrios Argyris, Dimitrios V. Papavassiliou, Alberto Striolo, Lloyd L. Lee & David R. Cole (2011): Interfacial water on crystalline silica: a comparative molecular dynamics simulation study, Molecular Simulation, 37:03, 172-195

To link to this article: http://dx.doi.org/10.1080/08927022.2010.513008

Molecular Simulation
Vol. 37, No. 3, March 2011, 172–195

Interfacial water on crystalline silica: a comparative molecular dynamics simulation study

Tuan A. Ho[a], Dimitrios Argyris[a], Dimitrios V. Papavassiliou[a], Alberto Striolo[a]*, Lloyd L. Lee[b] and David R. Cole[c]

[a]*School of Chemical, Biological, and Materials Engineering, The University of Oklahoma, Norman, OK 73019, USA;* [b]*Department of Chemical and Materials Engineering, California State Polytechnic University, Pomona, CA 91768, USA;* [c]*School of Earth Sciences, The Ohio State University, Columbus, OH 43210, USA*

(*Received 22 May 2010; final version received 21 July 2010*)

Understanding the properties of interfacial water at solid–liquid interfaces is important in a wide range of applications. Molecular dynamics is becoming a widespread tool for this purpose. Unfortunately, however, the results of such studies are known to strongly depend on the selection of force fields. It is, therefore, of interest to assess the extent by which the implemented force fields can affect the predicted properties of interfacial water. Two silica surfaces, with low and high surface hydroxyl density, respectively, were simulated implementing four force fields. These force fields yield different orientation and flexibility of surface hydrogen atoms, and also different interaction potentials with water molecules. The properties for interfacial water were quantified by calculating contact angles, atomic density profiles, surface density distributions, hydrogen bond density profiles and residence times for water near the solid substrates. We found that at low surface density of hydroxyl groups, the force field strongly affects the predicted contact angle, while at high density of hydroxyl groups, water wets all surfaces considered. From a molecular-level point of view, our results show that the position and intensity of peaks observed from oxygen and hydrogen atomic density profiles are quite different when different force fields are implemented, even when the simulated contact angles are similar. Particularly, the surfaces simulated by the CLAYFF force field appear to attract water more strongly than those simulated by the Bródka and Zerda force field. It was found that the surface density distributions for water strongly depend on the orientation of surface hydrogen atoms. In all cases, we found an elevated number of hydrogen bonds formed between interfacial water molecules. The hydrogen bond density profile does not depend strongly on the force field implemented to simulate the substrate, suggesting that interfacial water assumes the necessary orientation to maximise the number of water–water hydrogen bonds irrespectively of surface properties. Conversely, the residence time for water molecules near the interface strongly depends on the force field and on the flexibility of surface hydroxyl groups. Specifically, water molecules reside for longer times at contact with rigid substrates with high density of hydroxyl groups. These results should be considered when comparisons between simulated and experimental data are attempted.

Keywords: molecular dynamics; atomistic; force-field effects

1. Introduction

The understanding of aqueous solutions near charged surfaces continues to attract great attention due to fast advances in applications including nanofabrication [1], 'lab-on-chip' processes [2], water desalination [3–6], environmental science [7] and geochemistry [8].

Experimental investigations on interfacial water were carried out using, e.g. backscattering spectroscopy [9], quasi-elastic neutron scattering [10], attenuated total reflectance infrared spectroscopy [11], X-ray reflectivity measurements [12] and ultrafast infrared spectroscopy [13]. The experimental investigations are often enriched by theoretical studies conducted with the aid of computer simulations for structural [14–22] and dynamical [23–26] properties of interfacial water. This extensive body of literature supports the conclusion that interfacial water properties differ significantly from those observed in the bulk.

Previous studies, both from our group [25–27] and from others [19,28–31], have demonstrated how a solid flat silica surface perturbs the properties of interfacial water. Several force fields are available in the literature to describe silica and silica–water interactions [31]. We have previously implemented the force field proposed by Bródka and Zerda [32]. The CLAYFF force field [33] is recently being widely used, because it promises to be transferable and easily adaptable to study several mineral surfaces. The purpose of this work is to investigate how the model implemented to simulate the silica surface affects the results. Specifically, we address differences obtained when either the Bródka and Zerda or the CLAYFF force fields are implemented. We also address the effect of flexibility of surface hydroxyl groups on the results obtained via molecular simulation for the properties of interfacial water.

For our comparison to be effective, the silica surfaces simulated with the various force fields should be the same

*Corresponding author. Email: astriolo@ou.edu

ISSN 0892-7022 print/ISSN 1029-0435 online

DOI: 10.1080/08927022.2010.513008
http://www.informaworld.com

(i.e. same crystallographic plane, same density of hydroxyl groups, etc.). The silica surfaces used in this work were obtained by cutting the β-cristobalite SiO_2 crystal along the (1 1 1) crystallographic face. As discussed earlier [25–27], by cutting the cristobalite crystal at different depths, we can prepare surfaces with different densities of hydroxyl groups: the low hydroxyl density surface (LD) with 4.54 OH/nm^2 and the high hydroxyl density surface (HD) with 13.63 OH/nm^2. The exposed surface is created following the procedure originally proposed by Puibasset and Pellenq [29], and used in our prior reports [25–27]. No reconstruction of the surface, nor water dissociation at the surface is considered herein. Such effects could be studied using *ab initio* techniques [34–37]. In this paper, LD and HD surfaces are simulated utilising four classical force fields:

(1) LD-PER and HD-PER surfaces. As in our previous works [25–27], all non-bridging oxygen atoms

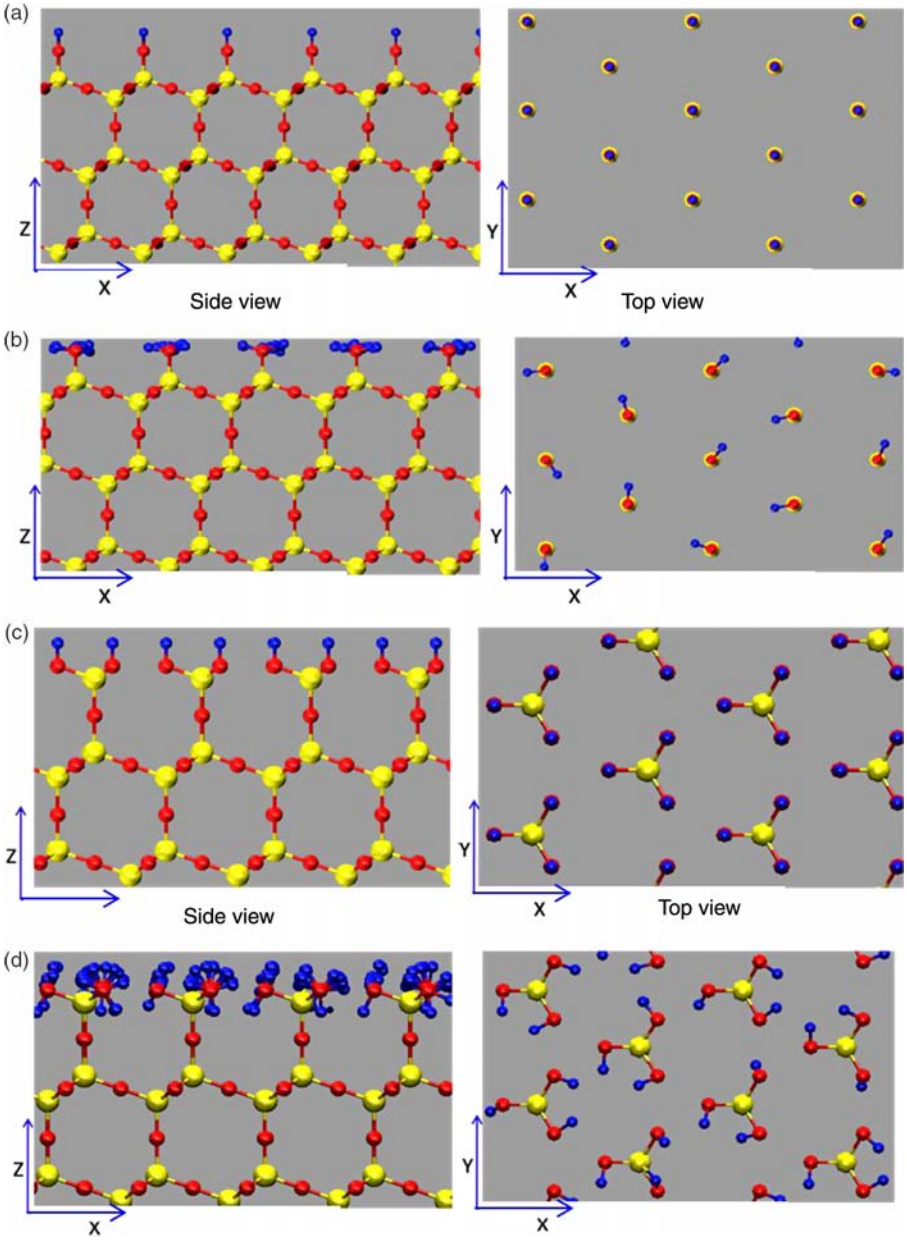

Figure 1. Side (left panels) and top (right panels) views of silica surfaces with low (top four panels) and high densities (bottom four panels) of hydroxyl groups (LD and HD surfaces, respectively). Panels (a)–(d) are for LD-PER, LD-RANDOM, HD-PER and HD-RANDOM surfaces, respectively. See Table 1 for nomenclature details. Blue, red and yellow spheres represent surface hydrogen, oxygen and silicon atoms, respectively (colour online). For clarity, in the top view (right panels), only silicon, oxygen and hydrogen atoms belonging to the surface silanol groups are shown.

are saturated with hydrogen atoms placed perpendicularly to the surface 1 Å away from the centre of the oxygen atoms. The surface hydrogens are kept rigid during the simulation. Silica–water interactions are simulated according to the Bródka and Zerda formalism [32]. Figure 1(a) and (c) illustrates the surface obtained with this force field. The figures present side and top views of LD and HD surfaces, respectively.

(2) LD-RANDOM and HD-RANDOM surfaces. All the non-bridging oxygen atoms are saturated with hydrogen atoms, 1 Å away from the non-bridging oxygen atoms. Although rigid, these hydrogen atoms are randomly oriented with respect to the solid substrate, while the Si–O–H angle always equals 109.47°. Figure 1(b) and (d) illustrates side and top views of LD and HD surfaces obtained implementing this force field, respectively. As in force field (1), silica–water interactions are simulated according to the Bródka and Zerda formalism [32].

(3) LD-CLAYFF and HD-CLAYFF surfaces. The surface hydrogen atoms are allowed to rotate during the simulations. These rotations occur on a plane parallel to the surface in the case of the LD surface (Figure 2(a)), and on a plane perpendicular to the Si-O vector in the case of the HD surface (Figure 2(b)). The O–H equilibrium distance is set to 1 Å and the S–O–H equilibrium angle to 109.47°[33]. The vibrations of surface hydrogen atoms are described according to the CLAYFF formalism [33].

(4) LD-CLAYFF-RIGID and HD-CLAYFF-RIGID surfaces. Silica–water interactions are described according to the CLAYFF force field [33], but all atoms in the solid substrate are rigid. The solid substrate was prepared by conducting the simulation as described in (3). After 3 ns of simulation, the coordinates of the surface hydrogen atoms were frozen and used for all subsequent production runs in the formalism (4). Silica–water interactions in force fields (3) and (4) are simulated according to the CLAYFF formalism [33].

In Table 1, we provide the nomenclature used in our discussion to refer to the different surfaces simulated, with the corresponding force fields.

2. Simulation details

The simulations were carried out using the canonical ensemble (*NVT*), where the number of particles (*N*), the simulation box volume (*V*) and the system temperature (*T*) are constant [38]. The system temperature was set at 300 K and controlled by a Nosé–Hoover thermostat with a relaxation time of 0.1 ps. The integration of the equations of motion was performed with the molecular dynamics package GROMACS [39–42] using the Leapfrog algorithm with a time step of 1 fs. All the results presented in this study were obtained after 0.5 ns of equilibration time. No drift in the total system energy was observed during at least the second half of the equilibration phase. The production time was 3 ns, during which the atomic positions were recorded every 200 time steps (0.2 ps) and used for further analysis.

In Figure 3, we show the side view of our simulation box. The *X* and *Y* simulation box dimensions are 104.7 and 100.8 Å, respectively. To maintain overall charge neutrality, some of the oxygen atoms on the last layer of each slab were removed. The slab thickness is 18.52 Å for LD and 20.58 Å for HD surfaces, respectively (greater than the cut-off distance, 9 Å). These thick solid slabs were required to prevent unphysical interactions between the incomplete layer of oxygen atoms and interfacial water molecules. The solid substrates were aligned parallel to the *X*–*Y* plane. Two identical slabs of the same substrate were set facing each other across the pore volume, thus yielding a slit-shaped pore. Water was inserted in the space between the two solid substrates. The distance between the two solid surfaces is $H = 101.3$ Å. The number of simulated

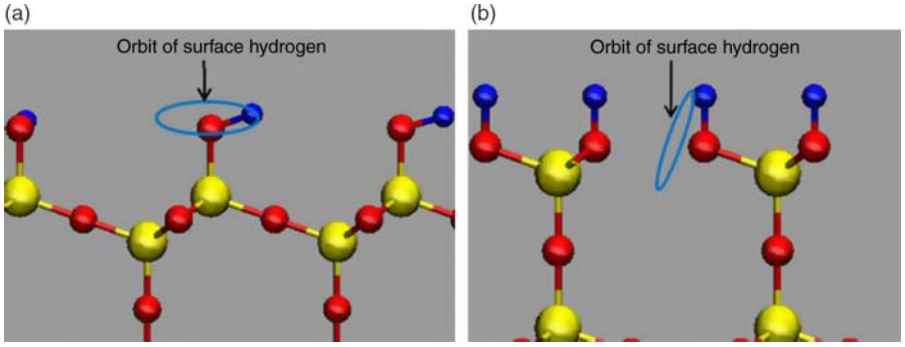

Figure 2. Orbit of surface hydrogen atom rotation on LD-CLAYFF (a) and HD-CLAYFF (b) surfaces when the CLAYFF force field is implemented.

Table 1. Nomenclature used to differentiate the solid substrates simulated herein.

Label	Hydroxyl density (OH/nm^2)	Force field
LD-PER	Low: 4.54	Bródka and Zerda [32]
LD-RANDOM	Low: 4.54	Bródka and Zerda [32]
LD-CLAYFF	Low: 4.54	CLAYFF [33]
LD-CLAYYF-RIGID	Low: 4.54	CLAYFF [33]
HD-PER	High: 13.63	Bródka and Zerda [32]
HD-RANDOM	High: 13.63	Bródka and Zerda [32]
HD-CLAYFF	High: 13.63	CLAYFF [33]
HD-CLAYFF-RIGID	High: 13.63	CLAYFF [33]

Note: The labels provided in the first column from the left are used throughout the text. The second and third columns provide the densities of hydroxyl groups on each surface, and the references for the force fields implemented to describe silica–water interactions, respectively.

water molecules was 12,250 for all simulations discussed below, except those conducted to assess the contact angles (details below). Bond length and angle in water molecules were kept fixed using the SHAKE algorithm [43]. Water was simulated according to the simple point charge extended (SPC/E) model [44], unless otherwise noted. Periodic boundary conditions were implemented along the *X*, *Y* and *Z* directions. The cut-off distance for all interactions is 9 Å, and corrections for long-range electrostatic potentials were treated using the particle-mesh Ewald method [38,45].

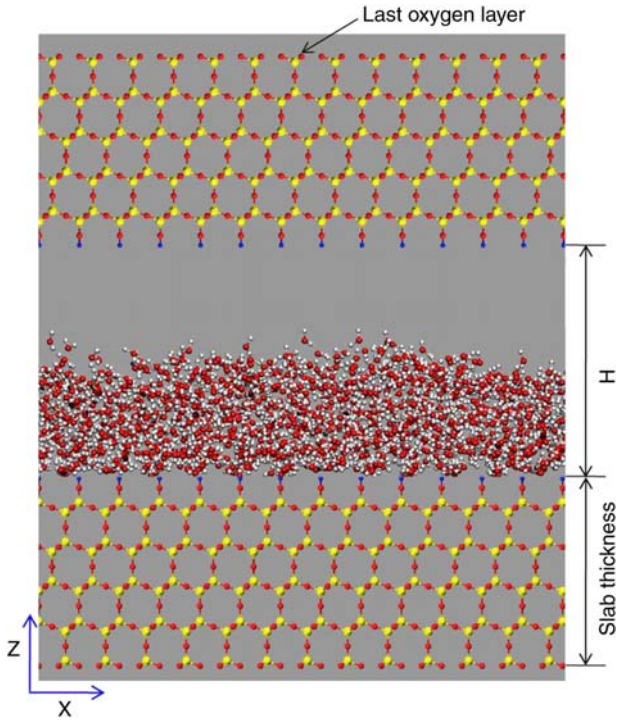

Figure 3. Side view of the simulation box. Blue, red, yellow and white spheres represent surface hydrogen, oxygen, silicon and water hydrogen atoms, respectively (colour online).

CLAYFF is a general force field [33] derived to enable molecular simulations of hydrated crystalline compounds and their interactions with fluids. Partial charges were assigned to the various atoms based on quantum mechanical calculations. Dispersive interactions were described by 12-6 Lennard-Jones (LJ) potentials, fitted to reproduce structural parameters known for a number of minerals. Bond stretch and bond-angle bend potentials were included only for surface hydroxyl groups. The CLAYFF force field was validated by comparing the structure of oxides, hydroxides and oxyhydroxides, as predicted via energy minimisation, to those available experimentally. Because the CLAYFF force field was derived based on the SPC model of water [46], it is expected that it should be used in combination with that water model to study solid–water interfaces. Our group has extensively used the SPC/E [44] model to study confined water. Thus, it is our interest to quantify how the results change when the water model is changed from SPC to SPC/E.

In the Bródka and Zerda force field [32], dispersive and electrostatic interactions are also described using 12-6 LJ parameters and partial charges as given in Table 2. Bródka and Zerda calculated the LJ potential parameters for bridging oxygen atoms from the Kirkwood–Muller formula [47], and for non-bridging oxygen atoms, they chose a collision parameter similar to that used for oxygen in water. They used the semi-empirical method PM3, as built in the HYPERCHEM program, to determine the partial charges (for details see Ref. [32]). The force field was initially used to study silica-acetone systems and it was successfully employed for the study of water in

Table 2. Force field parameters used in the simulations.

Force field	Site	σ (nm)	ε (kJ/mol)	q (e)
Bródka and Zerda [32]	Si	0.0000	0.00000	1.2830
	BO[a]	0.2700	1.91107	−0.6290
	nbO[a]	0.3000	1.91107	−0.5330
	H	0.0000	0.00000	0.2060
CLAYFF [33]	Si	0.3302	7.7007E-06	2.1000
	BO	0.3166	0.65020	−1.0500
	nbO	0.3166	0.65020	−0.9500
	H	0.0000	0.00000	0.4250
SPC/E water [38]	O	0.3166	0.65020	−0.8476
	H	0.0000	0.00000	0.4238
SPC water [39]	O	0.3166	0.65020	−0.82
	H	0.0000	0.0000	0.41

Note: In the first column, we provide the name of the force fields. For each atom (second column), we report σ and ε (12-6 LJ parameters) and point charges in third, fourth and fifth column, respectively. [a] bO and nbO stand for bridging and non-bridging oxygen atoms, respectively.

cylindrical silica pores by Gallo and co-workers [48,49]. The atoms of the silica substrate interact with water molecules by dispersive and electrostatic interactions [32].

To simulate water–solid interactions, LJ interaction parameters to describe the potentials between different atoms are needed, when either the CLAYFF or the Bródka and Zerda force fields are implemented. These interactions were treated as 12-6 LJ potentials with parameters determined by Lorentz–Berthelot mixing rules from those of the pure atoms [38]. In Table 2, we summarise the parameters used to implement all the force fields used in this work.

To assess macroscopic effects (namely, contact angles) due to the force fields at the water–silica interface, we simulated a small water droplet on all the substrates of Table 1. The simulated droplet was composed of 1000 SPCE/E water molecules. Although it is known that the contact angle obtained from atomistic simulations of small droplets depends significantly on the droplet size [50–52], our simulations for droplets composed by 1000 molecules are considered adequate for qualitatively assessing how the details of the implemented force fields affect macroscopic observations (e.g. we seek to estimate the hydrophobic as opposed to hydrophilic character of the simulated surfaces).

3. Results

When SPC water was simulated at contact with LD and HD surfaces, the results were practically indistinguishable from those discussed below for SPC/E water. We conclude that implementing either the SPC or SPC/E model to describe the structure properties of interfacial water has little effect on the results. In the remainder of this work, we only show results obtained when the SPC/E model of water was implemented. The explicit comparison between the results obtained implementing either SPC or SPC/E models for water is summarised in Appendix A.

3.1 Contact angles

To assess the macroscopic features of the simulated surfaces, we considered a drop of 1000 water molecules supported on the eight substrates. The results shown in Figures 4 and 5 are for LD and HD surfaces, respectively. The first difference between all the simulated systems is that as the density of the surface hydroxyl groups increases, going from the LD surfaces shown in Figure 4 to the HD surfaces shown in Figure 5, the substrates become more hydrophilic, as indicated by the shape of the water droplets. The water droplets wet the HD substrates (Figure 5), while bead up on the LD ones (Figure 4). Because of these effects, the most interesting differences due to the force field type are observed on the LD surfaces (Figure 4), where the contact angle changes significantly depending on the force field implemented. When the CLAYFF force field is implemented, the surfaces are more hydrophilic than when the Bródka and Zerda force field is applied (compare Figure 4(a) and (b) with Figure 4(c) and (d)). Surprisingly, the LD-PER surface, on which the surface hydroxyl groups are rigid and perpendicular to the substrate, is significantly less hydrophilic than the surface with randomly oriented, albeit rigid hydrogen atoms (LD-RANDOM) (compare Figure 4(a) with (b)). The Bródka and Zerda force field appears to attract water less strongly than the CLAYFF force field does, even when the substrate is maintained rigid (compare Figure 4(b) with (d)). Allowing for the mobility of the surface hydroxyl groups has little effect on the

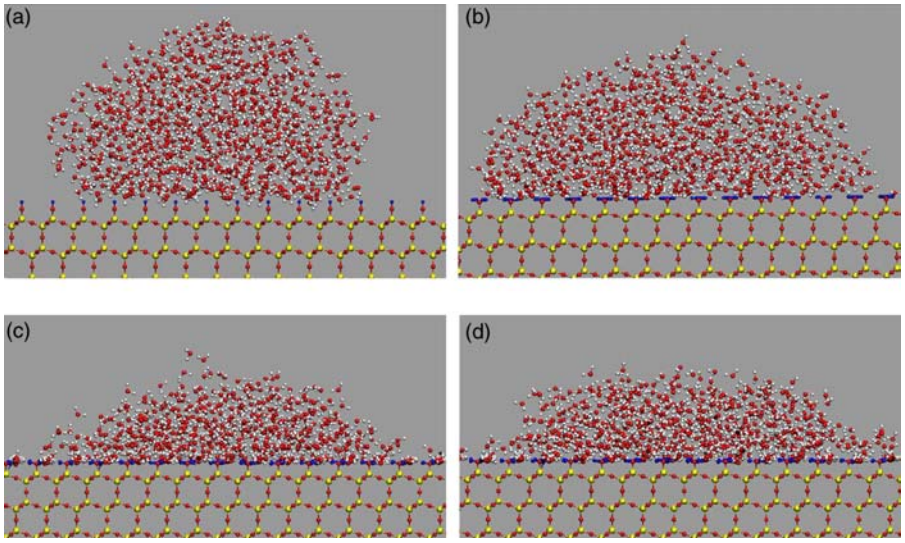

Figure 4. Representative simulation snapshots for one droplet of 1000 SPC/E water molecules equilibrated at 300 K on LD-PER (a), LD-RANDOM (b), LD-CLAYFF (c) and LD-CLAYFF-RIGID (d) surfaces. See Table 1 for details.

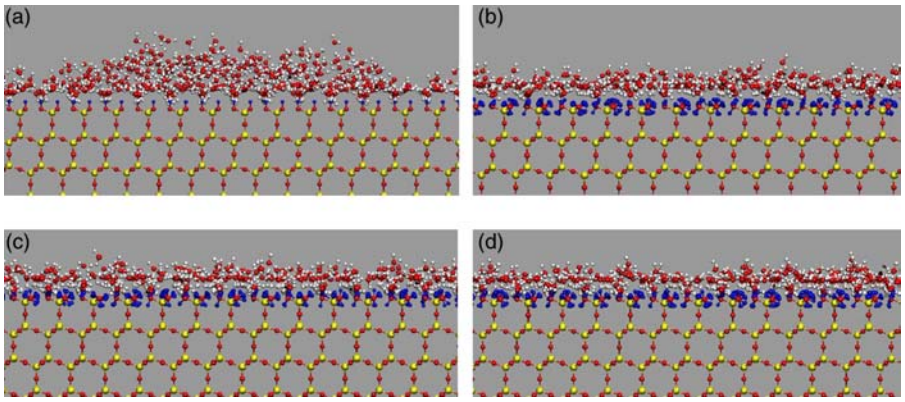

Figure 5. Representative simulation snapshots for one droplet of 1000 SPC/E water molecules equilibrated at 300 K on HD-PER (a), HD-RANDOM (b), HD-CLAYFF (c) and HD-CLAYFF-RIGID (d) surfaces. See Table 1 for details.

contact angle when the CLAYFF force field is implemented (compare Figure 4(c) with (d)).

3.2 *Atomic density profiles*

In Figure 6, we show the oxygen (a) and hydrogen (b) atomic density profiles for SPC/E water molecules as a function of the distance z from the LD surfaces. The reference $z = 0$ is the plane of non-bridging oxygen atoms of the bottom slab (see Figure 1). As observed for liquid water at contact with a number of solid substrates [9,14,15,23,24,53–55], our results show evidence of water structuring on the LD silica surface. It is, however, surprising that the various force fields affect the structure of interfacial water as strongly as it appears in Figure 6, when we remember that all surfaces are chemically similar, despite the differences in contact angle described in Figure 4. The position of atomic density peaks observed from the profiles in Figure 6 is given and labelled in Table 3. These labels are used throughout the paper. The results in Figure 6 indicate that the surface perturbs interfacial water up to 10–12 Å from the surface. At larger distances, the density of water is 0.0331/Å^3 which corresponds to bulk density. Our results indicate that the force field strongly affects the interfacial water structure and the orientation of water molecules near the surfaces. The results obtained on the LD surface with rigid, perpendicular surface hydrogen atoms (LD-PER, see Figure 1(a)) are extensively described in our prior publication [25]. In brief, the oxygen atomic density profile (blue curve in Figure 6(a)) shows one shoulder LAO-1 (see Table 3) at 2.15 Å, one pronounced peak LAO-2 at 3.15 Å and another, less pronounced peak LAO-3 at 6.00 Å (colour online). The LAO-1 shoulder, with intensity nearly equal to bulk density, suggests the

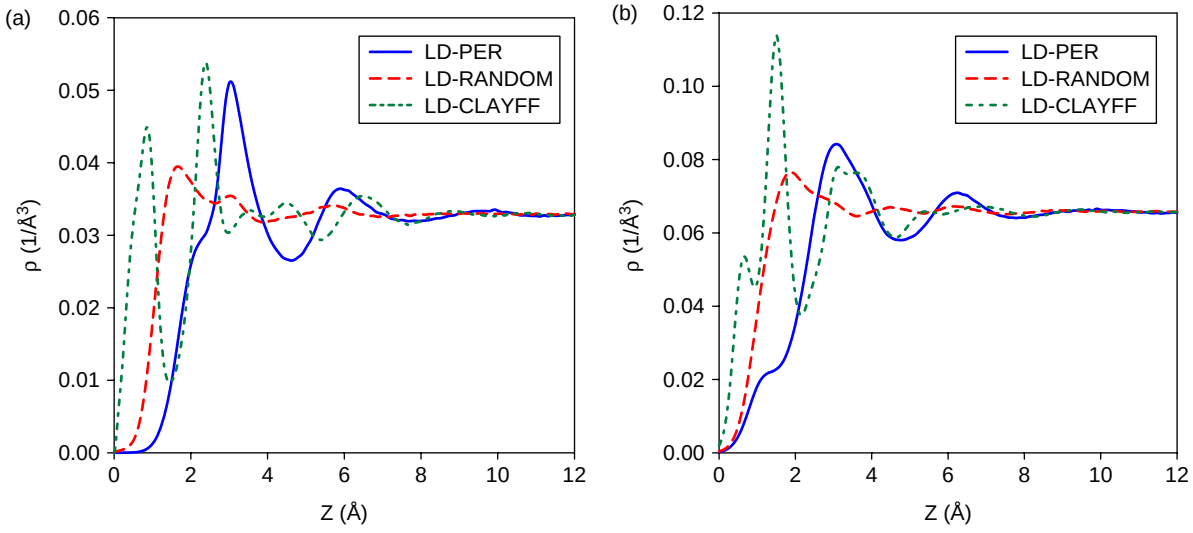

Figure 6. Oxygen (a) and hydrogen (b) atomic density profiles for SPC/E water molecules as a function of the distance z from the LD surfaces. The reference $z = 0$ is the plane of non-bridging oxygen atoms of the bottom slab (see Figure 3). This reference will be used throughout this work.

Table 3. Position of oxygen and hydrogen peaks as seen in the density profiles of Figure 6, with corresponding labels, obtained for SPC/E water simulated on LD surfaces at 300 K.

Surface	Oxygen peak (Å)	Hydrogen peak (Å)	Layer label
LD-PER	2.15	1.20	LAO-1/LAH-1
	3.15	3.15	LAO-2/LAH-2
	6.00	6.30	LAO-3/LAH-3
LD-RANDOM	1.75	1.85	LBO-1/LBH-1
	3.15		LBO-2
	5.75		LBO-3
LD-CLAYFF	0.95	0.75	LCO-1/LCH-1
	2.45	1.50	LCO-2/LCH-2
	3.55	3.25	LCO-3/LCH-3
	4.65	3.80	LCO-4/LCH-4
	6.55		LCO-5
LD-CLAYFF-RIDIG	0.95	0.75	LDO-1/LDH-1
	2.45	1.50	LDO-2/LDH-2
	3.55	3.25	LDO-3/LDH-3
	4.65	3.80	LDO-4/LDH-4
	6.55		LDO-5

presence of structured water close to the surface. The intense first peak, LAO-2 in Table 3, indicates that a large number of water molecules accumulate near the LD-PER surface. As the distance z increases, the effect of the surface on interfacial water weakens. We point out that the displaced position of the first peak (LAO-2) observed on the LD-PER surface may be indicative of the relatively hydrophobic character of that surface, as evidenced by the snapshot of Figure 4(a). Note however, that it remains difficult to correlate the molecular-level structure of interfacial water with macroscopic hydrophilic/hydrophobic characterisations, as recently discussed by Godawat et al. [56] and Voronov et al. [57].

When the surface hydrogen atoms are rigid, but randomly oriented (LD-RANDOM surface, red curve in Figure 6(a)), we observe a first weak oxygen peak LBO-1 at $z = 1.75$ Å and two less pronounced peaks at 3.15 and 5.75 Å. The first oxygen peak (LBO-1 in Table 3) is closer to the LD-RANDOM surface than the first oxygen peak LAO-2 is on the LD-PER surface. However, the intensity of the LBO-1 peak is much weaker than that of the LAO-2 peak. At distances larger than that at which the LBO-1 peak occurs, the water oxygen density decays to that of bulk water, as z increases. This feature is reminiscent of a structureless accumulation of water, possibly in contact with a rather hydrophobic substrate, in qualitative agreement with contact angle observations discussed in Figure 4. To explain the different position of the first oxygen peak observed on the two rigid LD substrates (blue vs. red curves in Figure 6(a)), we note that the average position of surface hydrogen atoms of LD-RANDOM surface with respect to the plane of non-bridging oxygen atoms ($z = 0$) is lower than that of LD-PER surface (see Figure 7). Although the O–H distance on the surface hydroxyl groups (0.1 nm) is less than the radius of the non-bridging oxygen atoms (see Table 2), this geometrical detail explains in part why the first layer of water molecules forms closer to the LD-RANDOM surface compared to the LD-PER surface.

When the surface hydrogen atoms are allowed to move by implementing the CLAYFF force field (green curve in Figure 6(a)), we observe two pronounced peaks at $z = 0.95$ and 2.45 Å, respectively, and three less pronounced peaks at $z = 3.55$, 4.65 and 6.55 Å. The first peak, LCO-1, is closer to the surface and far more pronounced compared to those observed on the other surfaces, indicating the accumulation of significant amounts of water close to the LD-CLAYFF surface. It is likely that this accumulation is due to largely favourable interactions between the substrate and the water molecules (i.e. evidence of hydrophilic character, in qualitative agreement with results discussed in Figure 4(c)), possibly established via the formation of extensive surface–water hydrogen bonds.

To complement the results for oxygen atomic density profiles, the atomic density profiles for water hydrogen atoms are presented in Figure 6(b). In the case of LD-PER surface (blue curve online), a shoulder LAH-1 is found at 1.2 Å. The corresponding hydrogen atoms are closer to the surface than the shoulder of oxygen atoms LAO-1, indicating that one of the two hydrogen atoms of some water molecules belonging to the LAO-1 shoulder has hydrogen-down orientation. The intense first hydrogen peak LAH-2, located at 3.15 Å, is found at the same position as the oxygen peak LAO-2, but it is nearly double

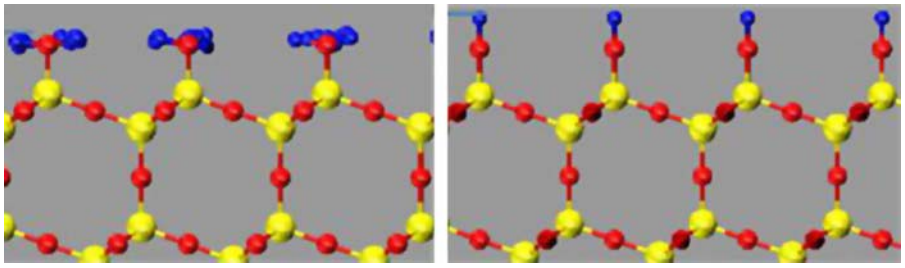

Figure 7. Position of surface hydrogen atoms with respect to the plane of non-bridging oxygen in LD-RANDOM and LD-PER surfaces (left and right panels, respectively).

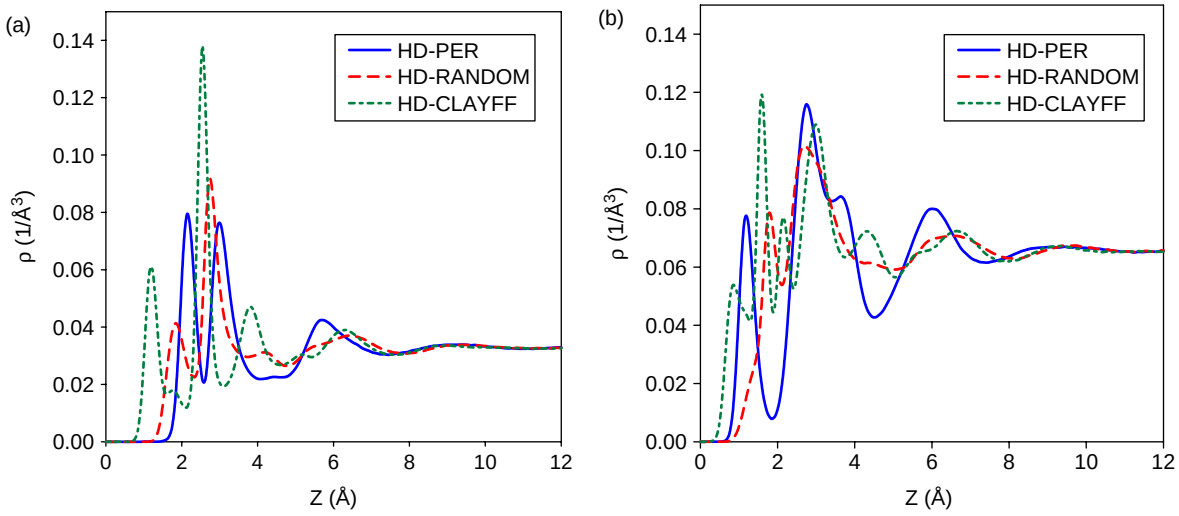

Figure 8. Oxygen (a) and hydrogen (b) atomic density profiles for SPC/E water molecules as a function of distance z from the HD surfaces. The reference $z = 0$ is the plane of non-bridging oxygen atoms of the bottom slab.

in intensity. Because the distance between LAH-2 and LAO-1 layer positions is 1 Å, our results suggest that approximately one half of the hydrogen atoms in layer LAH-2 belong to those water molecules whose oxygen atoms lay in the LAO-1 layer. The second half of the hydrogen atoms in layer LAH-2 probably belongs to those water molecules whose oxygen atoms accumulate in layer LAO-2. The orientation of the OH bond for the latter molecules is parallel to the surface. With respect to LD-RANDOM surface (red curve online), the first hydrogen peak LBH-1 is almost at the same position and has twice the intensity compared to the corresponding oxygen peak LBO-1, indicating hydrogen-parallel orientation for both hydrogen atoms belonging to each water molecule whose oxygen atom is in layer LBO-1. In the case of LD-CLAYFF surface (green curve online), the position and intensity of the first hydrogen peak LCH-1 are almost identical to those of the oxygen peak LCO-1, suggesting that one of the hydrogen atoms belonging to the water molecules whose oxygen atom is in the LCO-1 layer is parallel to the surface while the other extends away from it. The most pronounced hydrogen peak LCH-2, located at 1.50 Å, consists of hydrogen atoms belonging to the water molecules whose oxygen atoms are in the LCO-1 peak, plus hydrogen atoms of water molecules whose oxygen atoms belong to the LCO-2 layer. The latter water molecules, therefore, thrust one of their hydrogen atoms towards the surface, despite being rather far from it.

The differences just discussed between the results shown in Figure 6(a) and (b) suggest that implementing various force fields for the solid substrate affects not only the accumulation of water near the substrates, but also the orientation of interfacial water molecules. These microscopic observations complement the macroscopic contact angle predictions shown, albeit qualitatively, in Figure 4.

Analogous results were obtained near HD surfaces, summarised in Figure 8 as oxygen (a) and hydrogen (b) atomic density profiles for SPC/E water molecules. As expected, even the HD surfaces affect the structure of interfacial water, yielding peaks and valleys in the observed density profiles. The positions of the atomic density peaks observed in Figure 8 are given and labelled in Table 4. In all cases, the results show the formation of structured water at the solid–liquid interface, although pronounced differences in both peak intensity and location are observed when the different force fields are implemented. We found that the first oxygen peak on the HD-CLAYFF surface is closer to the surface than those found on HD-RANDOM and HD-PER surfaces.

Table 4. Position of oxygen and hydrogen peaks observed for water on HD surfaces (see Figure 8) with corresponding labels.

Surface	Oxygen peak (Å)	Hydrogen peak (Å)	Layer label
HD-PER	2.15	1.15	HAO-1/HAH-1
	2.95	2.75	HAO-2/HAH-2
	5.75	3.65	HAO-3/HAH-3
		6.05	HAH-4
HD-RANDOM	1.85	1.75	HBO-1/HBH-1
	2.75	2.75	HBO-2/HBH-2
	4.25		HBO-3/HBH-3
HD-CLAYFF	1.25	0.85	HCO-1/HCH-1
	2.55	1.65	HCO-2/HCH-2
	3.85	2.15	HCO-3/HCH-3
	6.35	3.05	HCO-4/HCH-4
HD-CLAYFF-RIGID	1.25	0.85	HDO-1/HDH-1
	2.55	1.65	HDO-2/HDH-2
	3.85	2.15	HCO-3/HDH-3
	6.35	3.05	HDO-4/HDH-4

This observation is rather surprising because macroscopically, as shown in Figure 5, our simulations predict little change on the properties of one water droplet on all the HD substrates. Interestingly, water molecules appear to be 'detached' from the HD-RANDOM surface, while they are strongly coordinated with the atoms of the HD-CLAYFF substrate. In Figure 9, we compare two snapshots (one for HD-RANDOM, left, and one for HD-CLAYFF, right) to highlight the different structure of interfacial water on the two surfaces. This difference is due to the strength of water–substrate interaction potentials. It appears that the Bródka and Zerda force field yields a surface that is less attractive to water than the CLAYFF force field, as already observed for the contact angle on the LD surfaces (see Figure 4). Visual inspection of the snapshots in Figure 9 suggests that the instantaneous distribution of the surface hydrogen atoms on the HD-RANDOM and CLAYFF substrates is not very different, even though the hydrogen atoms on the former surface are not allowed to move, while they rotate according to the CLAYFF force field on the latter surface. Therefore, it is likely that the different water–silica interactions, rather than the different surface flexibility, are responsible for the differences in Figure 9. The first oxygen shoulders on LD-PER and LD-RANDOM surfaces become fully developed peaks on HD-PER and HD-RANDOM surfaces, respectively, because of the larger density of surface hydroxyl groups. This suggests that a large amount of water accumulates near the surface because of the increased hydroxyl density. The second and third peaks on HD-PER and HD-RANDOM surface are closer to the surface than on LD-PER and LD-RANDOM, respectively, proving that increasing hydroxyl density increases the surface hydrophilicity. The latter observations are consistent with the differences in contact angle discussed in Figures 4 and 5, where we showed that increasing the surface density of the hydroxyl groups in the surfaces considered renders the surface much more hydrophilic.

Comparing the results obtained on HD vs. LD surfaces, we observe that the second oxygen peak on the HD-CLAYFF surface becomes much more intense than the corresponding peak on LD-CLAYFF. This indicates that many water molecules (four times more than in an equal volume of bulk water) concentrate at 2.55 Å from the HD-CLAYFF surface (HCO-2 layer highlighted in Figure 10). Visual inspection of simulation snapshots suggests that water molecules belonging to the HCO-2 layer can assume a number of favourable orientations: (a) they can project one hydrogen atom towards the solid substrate, (b) they can form hydrogen bonds with water molecules closer to the substrate and (c) they can form hydrogen bonds with water molecule further from the substrate. All three orientations favour the accumulation of water on the HCO-2 layer, and lead to the intense density peak. Because the intensity of the HCO-2 peak does not depend on the mobility of the surface hydroxyl groups (results obtained on the HD-CLAYFF-RIGID surface are indistinguishable from those obtained on the HD-CLAYFF one), the accumulation of water observed on the silica surface is mostly due to surface–water interactions and much less to the flexibility of the surface hydroxyl groups.

To complement the oxygen density profiles, in Figure 8(b), the atomic density profiles for hydrogen atoms are shown for different HD surfaces. On the HD-PER surface (blue curve), the first hydrogen peak, HAH-1, is located at 1.15 Å. This distance is 1 Å closer to the surface than that of the oxygen peak HAO-1, suggesting that one of the two hydrogen atoms of water belonging to HAO-1 layer has hydrogen-down orientation. With respect to HD-RANDOM surfaces, both hydrogen peaks HBH-1 and HBH-2 are located at the same position of the corresponding oxygen peak HBO-1 and HBO-2. However,

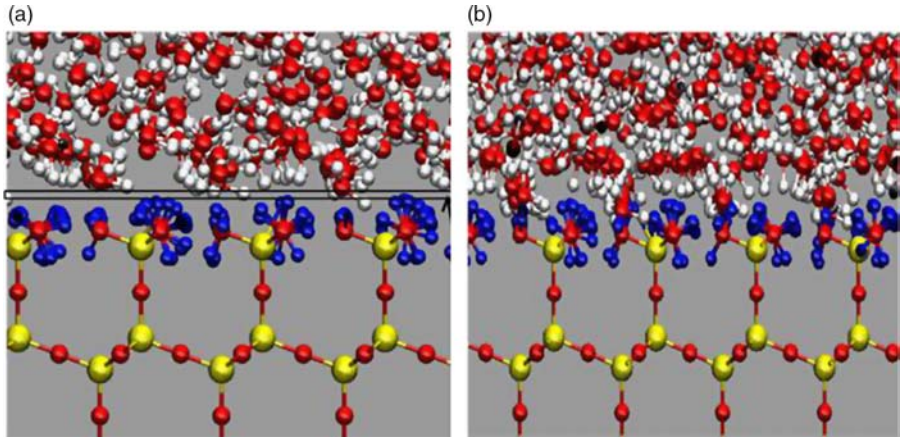

Figure 9. Simulation snapshots of hydrated (a) HD-RANDOM and (b) HD-CLAYFF surfaces. The black rectangle on the left panel highlights a volume depleted of water molecules. The same volume is completely filled with water molecules in panel (b).

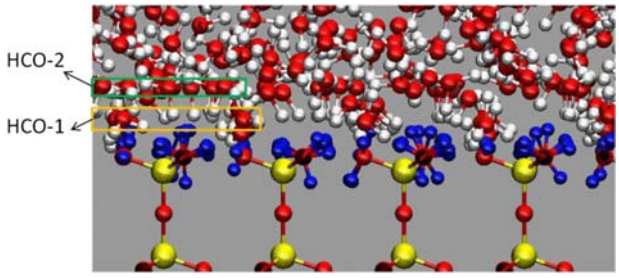

Figure 10. Representative simulation snapshot of hydrated HD-CLAYFF surface. Yellow and green rectangles highlight the first HCO-1 and second HCO-2 water layers, respectively (colour online).

the intensity of the hydrogen peaks is twice that of the oxygen peaks, suggesting that all the water molecules that belong to these layers have hydrogen-parallel orientation (i.e. the OH vector is parallel to the surface). In the case of HD-CLAYFF surface (green curve online), the first hydrogen peak is closer to the surface than the corresponding oxygen peak, and the two peaks have nearly the same intensity. The discussion could be continued to analyse each peak observed in the density profiles. For brevity, we only provide a representative simulation snapshot (Figure 10), to illustrate the structure of interfacial water on the HD-CLAYFF surface.

In Figures 4 and 6, we do not report the results obtained on the LD-CLAYFF-RIGID and HD-CLAYFF-RIGID substrates because they are indistinguishable compared to those obtained on the LD-CLAYFF and HD-CLAYFF surfaces, respectively. We conclude that the atomic density profiles do not depend on the movement of surface hydrogen atoms, but strongly depend on the silica–water interaction potentials when the CLAYFF

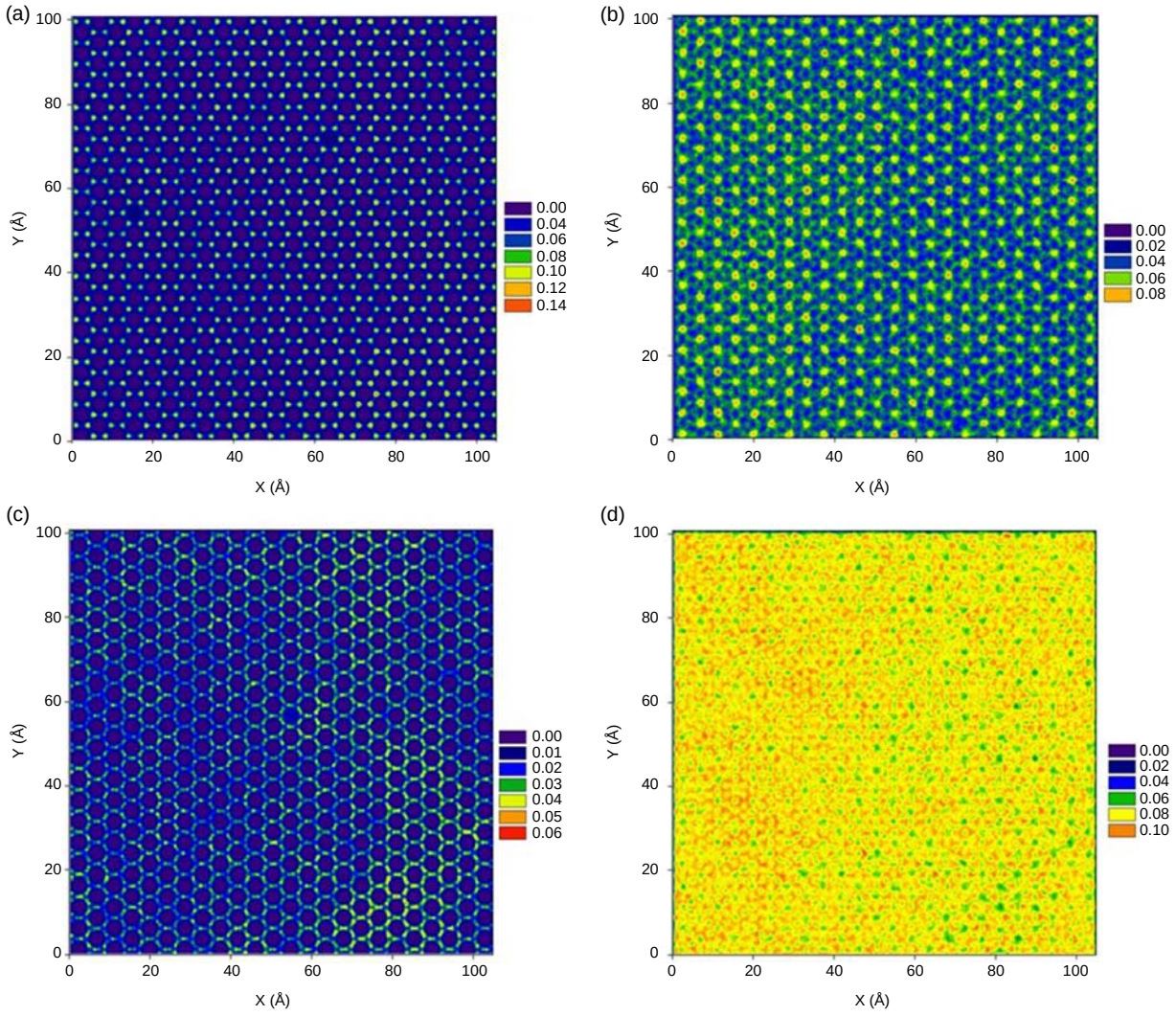

Figure 11. Surface density distributions for oxygen and hydrogen atoms of interfacial water near LD-PER surfaces (see Table 1). Panels (a)–(d) represent results for LAO-1, LAO-2, LAH-1 and LAH-2 peaks, respectively. See Table 3 for peak position. Surface density distributions are expressed in number of atoms per $Å^3$.

force field is implemented. This observation corroborates the qualitative comparison of contact angles provided in Figures 4 and 5.

3.3 Surface density distributions

To relate the morphological properties of our solid substrates to differences observed in the density of interfacial water, we calculate the surface density distribution of oxygen and hydrogen atoms on planes parallel to the substrate and centred on the density profiles peaks. The thickness of these planes is 1 Å. More computational details about these calculations can be found in our prior publication [25].

In Figure 11(a) and (b), we provide the surface density distribution of oxygen atoms corresponding to LAO-1 and LAO-2 layers, respectively. The high density areas in the contour plot of Figure 11(a) indicate a highly structured first oxygen layer. Water molecules concentrate above the vertices of the hexagons formed by six silicon atoms on the surface (see Figure 12 for details). This suggests that the structure of the first layer of water molecules strongly depends on the crystal structure of the underlying substrate, as previously observed [25]. The results in Figure 11(b) also indicate a well structured second water layer. The oxygen atoms belonging to this layer are located 1 Å above the centre of the hexagons highlighted in Figure 12. In Figure 11(c) and (d), we show the surface density distribution of hydrogen atoms belonging to LAH-1 and LAH-2 layers, respectively. As we discussed in Section 3.2, the water molecules whose oxygen atom belongs to the LAO-1 layer assume a hydrogen-down orientation with respect to the surface. As a consequence, the hydrogen atom distribution in layer LAH-1 is very similar to the oxygen atom distribution in layer LAO-1 (compare Figure 11(a) with (c)). About one half of the hydrogen atoms belonging to layer LAH-2 belong to the water molecules whose oxygen atoms are located in layer LAO-1. The rest of the LAH-2 hydrogen atoms belong to the water molecules whose oxygen atoms are found in layer LAO-2. Because of this multiple source, the hydrogen atoms in layer LAH-2 show a rather uniform in-plane distribution (see Figure 11(d)).

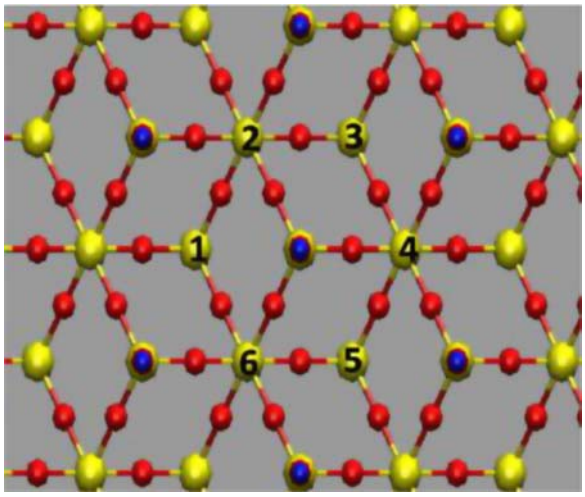

Figure 12. Hexagon formed by silicon atoms of LD-surface. The numbers present six vertices on the hexagon. Only surface atoms are shown for clarity.

In Figure 13, we provide the surface density distribution correspondent to the first oxygen layer LBO-1 (a), and the first hydrogen layer LBH-1 (b) on LD-RANDOM surfaces. The density distribution on the LBO-1 layer resembles that found on the LD-PER surface (see Figure 11(a)), although a number of imperfections emerge in the hexagonal distribution of oxygen atoms on the LD-RANDOM surface, reflecting the random orientation of the surface hydrogen atoms. More pronounced are the differences between the hydrogen atom density distribution in layer LBH-1 (Figure 13(b)) and that found in layer LAH-1 (Figure 11(c)). It appears that, because the surface hydrogen atoms are randomly oriented on the LD-RANDOM surface, the water molecules on the first adsorbed layer assume a variety of different orientations, yielding a distribution of water hydrogen atoms that lacks long-ranged order, as shown in Figure 13(b). This observation is reflected in rather short-ranged structuring of interfacial water near the surface, as shown in Figure 6.

The most interesting results were found in the case of surface density distributions on the LD-CLAYFF surface, where the surface hydrogen atoms are allowed to rotate. In Figure 14(a), we show the surface density distribution of the surface hydrogen atoms (notice that, for clarity, the scale of panel (a) is enlarged compared to that of the other panels in Figure 14). The high density areas, corresponding to the location of vertices 1, 3 and 5 of the hexagon formed by surface silicon atoms (Figure 12), indicate the preferential position of these surface hydrogen atoms. In Figure 14(b), we show the surface density distribution of the oxygen atoms found in layer LCO-1. Clearly, our results provide evidence for highly structured interfacial water, dictated by hydrogen bonds formed between interfacial water and surface hydroxyl groups. The water molecules preferentially accumulate on areas correspondent to the vertices 1, 3 and 5 of the hexagon formed by surface silicon atoms, highlighted in Figure 12. This suggests that water molecules accumulate where the surface hydrogen atoms are, implying the formation of strong hydrogen bonds between surface hydrogen atoms and water oxygen atoms. Figure 14(c) and (d) show the density distribution of oxygen atoms belonging to LCO-2 and LCO-3 layers, respectively. In the LCO-2 layer, the oxygen atoms distribute in circles whose centre is the centre of the silicon hexagons highlighted in Figure 12. This suggests that the movement of surface hydrogen

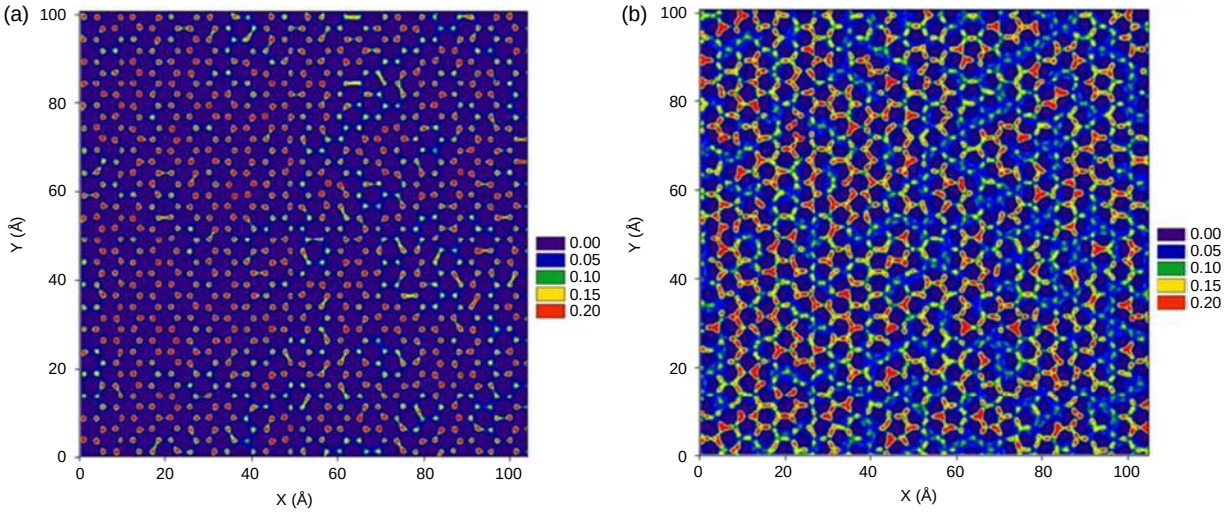

Figure 13. Surface density distribution of oxygen atoms in layer LBO-1 (a) and hydrogen atoms in layer LBH-1 (b) on the LD-RANDOM surface. See Table 3 for details on peak position. Surface densities are expressed in number of atoms per $Å^3$.

atoms, allowed by the CLAYFF force field, affects the distribution of water molecules belonging to the second oxygen layer. Far from the surface, the effect becomes weaker, although the oxygen atoms still accumulate on the vertices of the surface hexagons. Comparison between the surface distributions of Figure 14 with those shown in Figure 11 suggests that when the CLAYFF force field is implemented, the perturbation on the water structure extends further from the surface, as also demonstrated by the density profiles of Figure 6. The correlation between the density distribution of surface hydrogen atoms (Figure 14(a)) and the distribution of interfacial water molecules corroborates our earlier hypothesis according to which favourable surface–water interactions, manifested by hydrogen bonds, are responsible for the pronounced accumulation of water on the LD-CLAYFF surface, as discussed in Figure 6.

In Figure 15, we show the surface density distribution of the first and second hydrogen layers LCH-1 (a) and LCH-2 (b) on the LD-CLAYFF surface. Because each hydrogen atom in layer LCH-1 belongs to one water molecule whose oxygen lies in layer LCO-1, it is not surprising that the distribution of hydrogen atoms within the LCH-1 layer on the $(X–Y)$ plane is very similar to the distribution of oxygen atoms in layer LCO-1. The in-plane density distribution in layer LCH-2 shows circles and dots. Those two features can be explained by analysing the structure of interfacial water on the LD-CLAYFF surface. Hydrogen atoms in layer LCH-2 belong, in part, to the water molecules whose oxygen atoms are found in layer LCO-1 (these hydrogen atoms are likely to distribute on three vertices of the hexagon of Figure 12), and also to the water molecules whose oxygen atoms are located in layer LCO-2 (these hydrogen atoms are likely to distribute on the LCH-2 layer yielding circles clearly observable in the contour plot of Figure 15(b)).

In Figure 16, we provide the surface density distributions of oxygen atoms belonging to LDO-1 (a) and LDO-2 (b) layers on the LD-CLAYFF-RIGID surface. These results are totally different compared to those obtained on the LD-CLAYFF surface (Figure 14(b) and (c)), although the atomic density profiles for water oxygen and hydrogen atoms away from these surfaces are essentially identical (see Figure 6). The different results observed for the in-plane density distributions are due to the flexibility of surface hydroxyl groups, which is accounted for on the LD-CLAYFF substrate, but not on the LD-CLAYFF-RIGID surface. Our results suggest that the structure of water observed on the LD-CLAYFF surface (details in Figure 14) is very dynamic, and that the mobility of the surface hydroxyl groups is responsible for local fluctuations of interfacial water. When we freeze the surface hydroxyl groups, yielding the LD-CLAYFF-RIGID substrate, we essentially reduce the density fluctuations of interfacial water and we stabilise the structure of interfacial water evidenced by the contour plots shown in Figure 16.

The detailed analysis of in-plane atomic distributions obtained for interfacial water on the silica surfaces with high density of hydroxyl groups is discussed in detail in Appendix B. As expected, quantitative comparison yields strong differences when compared to the result just discussed because of the different density of surface hydroxyl groups. Further careful analysis of the simulation results shows that the details of the implemented force fields are important in determining the structural properties of interfacial water, although the differences observed when different force fields are implemented are more pronounced for LD than for HD surfaces.

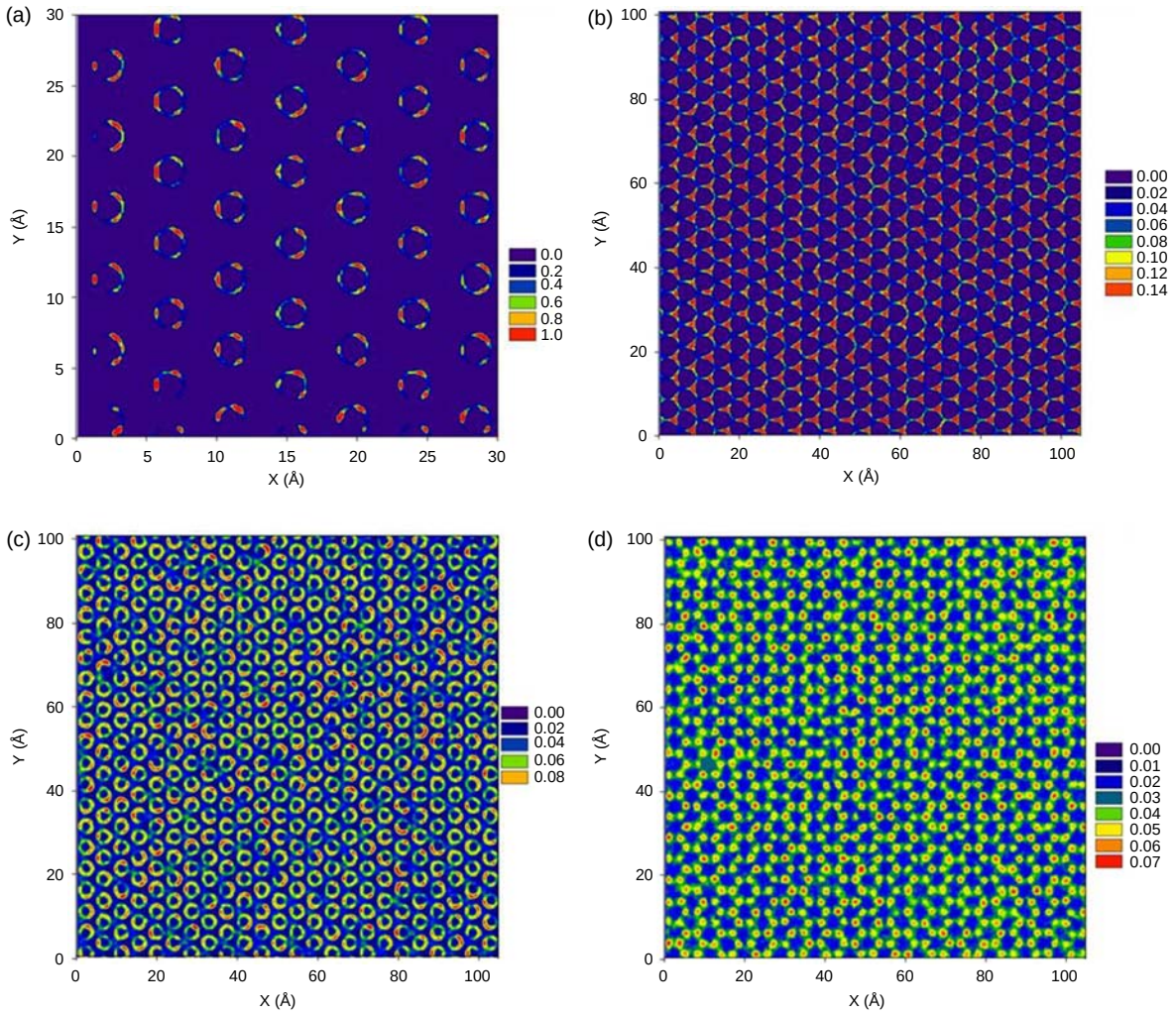

Figure 14. Surface density distribution of surface hydrogen atoms (a), oxygen atoms belonging to LCO-1 (b), LCO-2 (c) and LCO-3 (d) peaks on the LD-CLAYFF surface. See Table 3 for details on peak position. Note that, for clarity, an enlargement of the (*X*,*Y*) plane, rather than the entire surface, is provided in panel (a). Surface densities are expressed in number of atoms per $Å^3$.

3.4 Hydrogen-bond density profiles

The results from atomic density profiles and surface distributions discussed so far suggest that strongly structured water molecules accumulate close to each simulated surface. This may lead to the formation of hydrogen bonds among interfacial water molecules. In this section, we observe the resultant water–water hydrogen bond network as a function of the distance z from the surfaces. One hydrogen bond was identified using the geometric criterion proposed by Marti [58]. The position of each hydrogen bond was considered as the middle between the hydrogen of the donor and the oxygen of acceptor molecules. Similar definitions were introduced in Ref. [3]. The results shown in Figure 17 are the hydrogen bond density as a function of the distance z from LD (panel (a)) and HD surfaces (panel (b)). In the case of the LD-PER surface (blue curve online), the hydrogen-bond density peaks at $z = 3.1$ Å, corresponding to the LAO-2 and LAH-2 peaks found in the atomic density profiles (see Table 4). This suggests that a large number of hydrogen bonds form among water molecules whose oxygen atoms belong to the LAO-2 layer. On the LD-RANDOM surface (red curve online), we found a broad peak located at 2.7 Å, which lies in between LBO-1 and LBO-2 oxygen peaks. This indicates that a complicated hydrogen bond network forms among water molecules belonging to LBO-1 and LBO-2 layers, suggesting that water–water hydrogen bonds are responsible for extending the perturbation of interfacial water molecules further from the solid substrate. The hydrogen bond density profile on LD-CLAYFF surface (green curve online) is characterised by a shoulder at 2 Å and two peaks 2.45 and 2.95 Å. The shoulder indicates that a few hydrogen bonds form among water molecules whose oxygen atoms are confined within

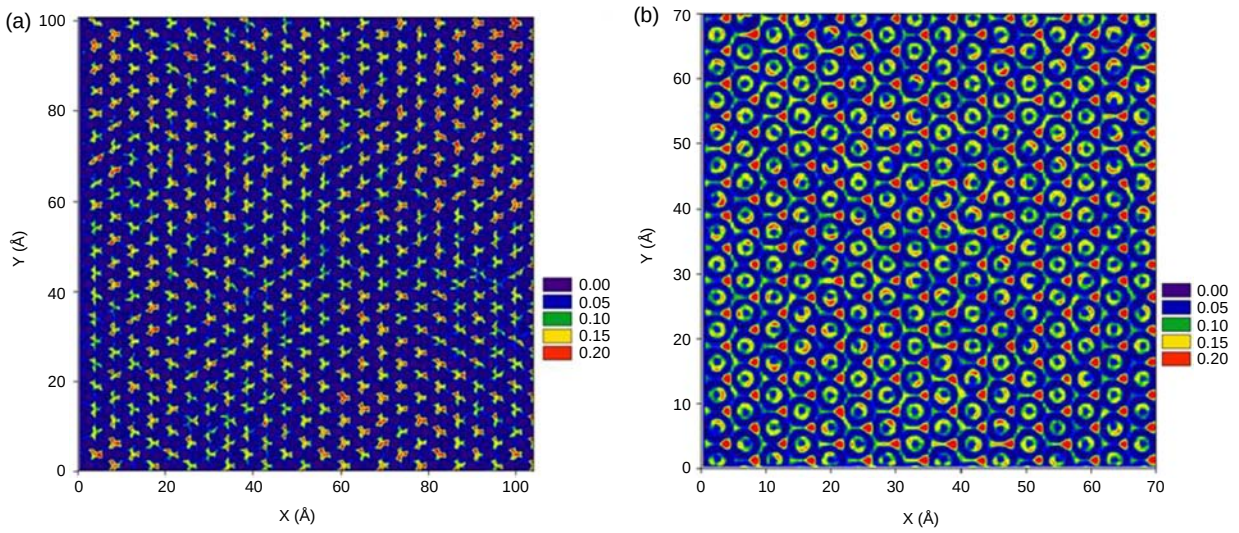

Figure 15. Surface density distribution of hydrogen atoms on LD-CLAYFF surface. Panels (a) and (b) are for LCH-1 and LCH-2 layers, respectively. See Table 3 for details on peak position. Surface densities are expressed in number of atoms per Å^3.

peaks LCO-1 and LCO-2. The hydrogen bond peak at 2.45 Å is at the same position than the second oxygen peak LCO-2, suggesting the formation of hydrogen bonds among water molecules whose oxygen atoms belong to that layer. Similar detailed comparison could be repeated for interfacial water on the silica surfaces with high density of hydroxyl groups (right panel of Figure 17). For brevity, we omit such discussion.

Despite all the differences discussed above, as well as the different atomic density profiles shown in Figure 6, it is surprising to note that the hydrogen bond density profile is very similar on all surfaces considered in Figure 17. These similarities suggest that the interfacial water molecules rearrange so as to maximise the number of water–water hydrogen bond, and this tendency compensates for different water structuring due to the solid substrates. The quantification of the density of hydrogen bonds of water near a substrate is important for developing thermodynamic models for describing, e.g. protein folding and aggregation [59].

3.5 *Residence time*

We also calculated the residence correlation function $C_R(t)$ of water molecules in a particular layer – i.e. how long water molecules stay at the interface. A 1-Å thickness slab

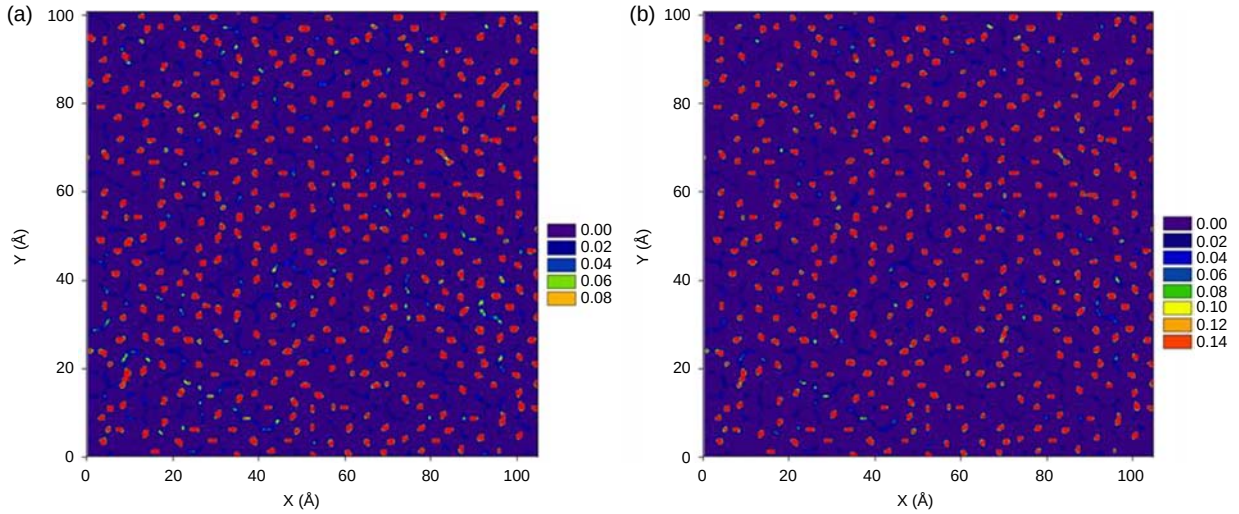

Figure 16. Surface density distributions of oxygen atoms belonging to LDO-1 (a) and LDO-2 (b) layers on LD-CLAYFF-RIGID surface. See Table 3 for details on peak position. Surface densities are expressed in number of atoms per Å^3.

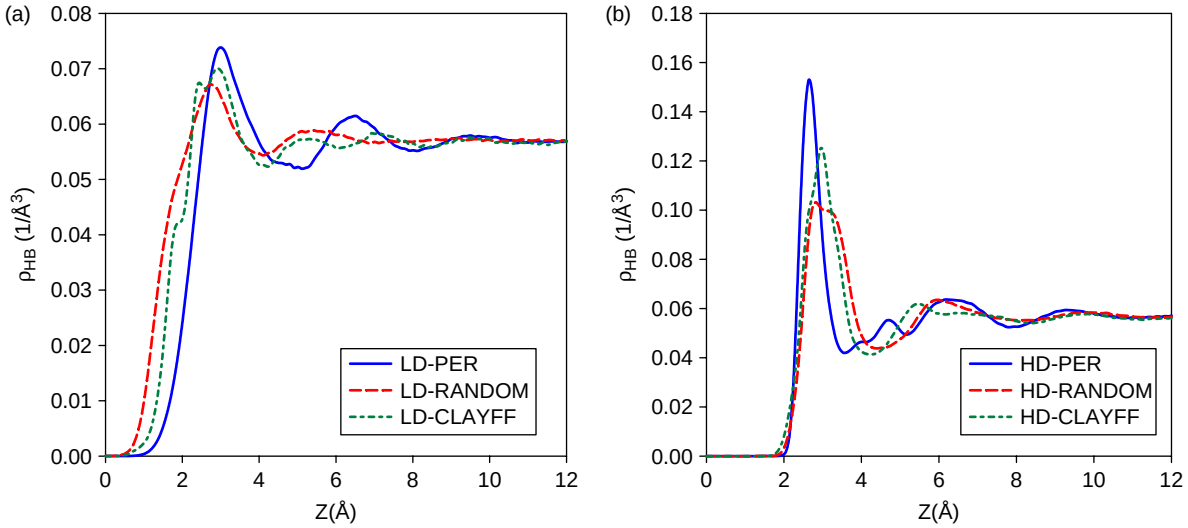

Figure 17. Hydrogen-bond density profiles as a function of distance z from LD (panel a) and HD surfaces (panel b). Blue, red and green curves represent the results obtained by implementing different force fields for the silica substrate (see Table 1 for details).

was considered and centred on the peaks of oxygen atomic density profiles (see Tables 3 and 4 for details). The residence correlation function was then quantified as [60]

$$C_R(t) = \frac{\langle O_w(t)O_w(0)\rangle}{\langle O_w(0)O_w(0)\rangle}, \quad (1)$$

where the angular brackets indicate ensemble averages. In Equation (1), the term $O_w(t)$ discriminates whether water molecule w belongs to the layer of interest at time t. If water molecule w belongs to the layer of interest at time $t = 0$, then $O_w(t = 0) = 1$. O_w remains equal to 1 as long as the water molecule remains in the layer, but becomes 0 when the molecule leaves the layer. After one water molecule leaves the layer of interest, O_w remains equal to 0 even if the molecule returns to the observed layer. Therefore, the autocorrelation function C_R is a measure of the time spent, on average, by the interfacial water molecules within each interfacial layer. The faster C_R decays from 1 to 0, the shorter the molecules reside at the interface.

In Figure 18, we show the correlation function $C_R(t)$ for water on LD surfaces. In both LD-PER (a) and LD-RANDOM (b) surfaces, the correlation function decays quickly. After 4 ps, no water molecule was found in the layers considered. However, for LD-CLAYFF surface (c), the residence time is longer for both layers LCO-1 (blue curve online) and LCO-2 (red curve online). These results are found also for water on HD surfaces (Figure 19).

Qualitatively, these results agree with our previous observations regarding contact angles and density distribution. According to our previous analysis, the CLAYFF force field yields silica substrates that attract water molecules more strongly than the Bródka and Zerda force field does. The results in Figure 18 and those in Figure 19 suggest that water molecules remain in contact with the more strongly attracting substrates longer than they do on less attractive ones. This observation is in

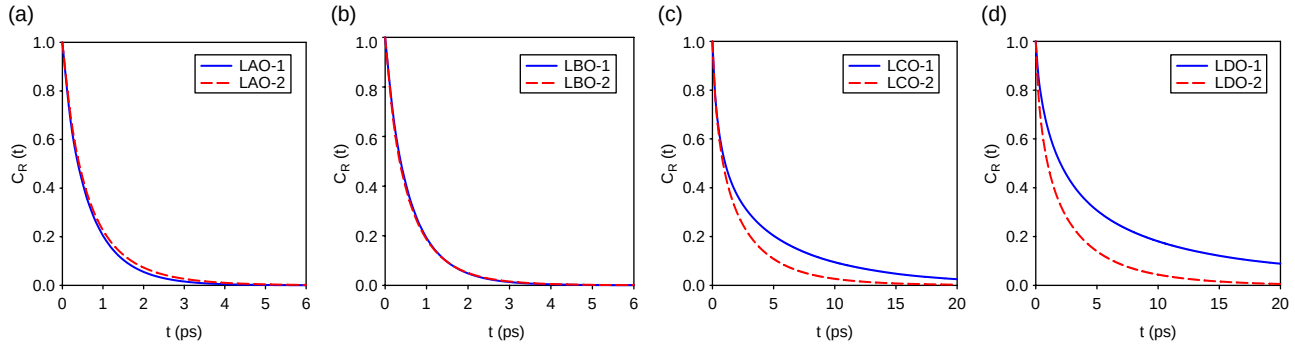

Figure 18. Residence correlation functions for oxygen atoms in various layers on LD-PER (a), LD-RANDOM (b), LD-CLAYFF (c) and LD-CLAYFF-RIGID (d) surfaces. See Table 3 for details on peak position.

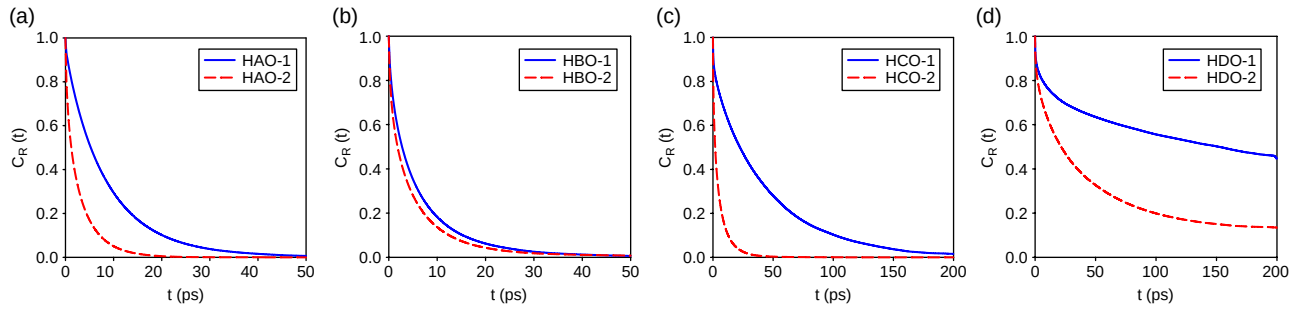

Figure 19. Residence correlation functions for oxygen atoms in various layers on HD-PER (a), HD-RANDOM (b), HD-CLAYFF (c) and HD-CLAYFF-RIGID (d) surfaces. See Table 4 for details on peak position.

qualitative agreement with the density fluctuations results used by Garde and co-workers [56] to discriminate between hydrophobic and hydrophilic surfaces. All prior observations within this work have shown little effect due to the flexibility of the surface hydroxyl groups on the reported results. On the contrary, results in Figure 18 and in Figure 19 show that when the surface hydroxyl groups are maintained rigid, interfacial water molecules remain in contact with the solid surface for long times (compare panels (d), obtained on the CLAYFF-RIGID surfaces, to panels (c), obtained on CLAYFF substrates, for both LD and HD surfaces). This observation is consistent with our description of the in-plane density distributions (Figure 16), which indicates that the rigidity of the surface hydroxyl groups may lead to less pronounced density fluctuations for contact water. In Section 3.4, we mentioned that the first layer of oxygen atoms LCO-1 forms the hydrogen bonds with surface hydrogen atoms. These hydrogen bonds depend on the flexibility of surface hydrogen atoms. When surface hydrogen atoms move, the hydrogen bonds break and the water molecules can easily move away from the interface. The effect of the flexibility of surface hydrogen atoms on residence time is more evident in the case of water on HD surface (Figure 19(c) vs. Figure 19(d)).

The analysis for the dynamical properties of interfacial water on the various substrates considered herein demonstrates that appropriately accounting for not only water–substrate interactions (we have compared the Bródka and Zerda to the CLAYFF force field), but also for the mobility of the surface hydroxyl groups (we have compared rigid vs. flexible substrates) is important for correctly describing both structural and dynamical properties of interfacial water.

4. Conclusions

The molecular structure of interfacial water on different silica surfaces was investigated using molecular dynamics simulations. Two silica surfaces, with LD and HD, were described under four formalisms different in the orientation and flexibility of surface hydroxyl groups and water–silica interactions. The interaction between atoms of silica surface and water molecules was described by either the CLAYFF or the Bródka and Zerda force fields. We calculated contact angles, atomic density profiles, surface density distribution, hydrogen bond density profiles and residence time for water at contact with all the simulated substrates. No significant differences were observed when either the SPC or the SPC/E models of water were implemented.

Our results show that as the density of surface hydroxyl groups increases, the substrates become more hydrophilic. At constant density of surface hydroxyl groups, the CLAYFF force field yields more hydrophilic substrates than the Bródka and Zerda one does. This results in different contact angles, particularly noticeable on surfaces with low density of hydroxyl groups, and also on different distributions of water molecules away from the surfaces. The in-plane distribution of water molecules and the related orientation of interfacial water strongly depend on the model implemented to simulate the surface, although no apparent correlation is found between macroscopic hydrophobic/hydrophilic character and microscopic details, in qualitative agreement with recent results reported by Garde and co-workers [56]. The network of water–water hydrogen bonds near the solid substrates does not seem to depend strongly on the force field implemented to simulate the solid, although the density of surface hydroxyl groups seems to strongly influence the density of water–water hydrogen bonds near the surface, presumably because of a competition between surface–water and water–water hydrogen bonds. In general, allowing for the flexibility of the surface hydroxyl groups does not seem to perturb significantly the structure of interfacial water. However, our results clearly show that when the surface hydroxyl groups are allowed to vibrate, water molecules remain next to the solid substrate for shorter times than when the surface hydroxyl groups are rigid, presumably because as the surface hydroxyl groups rotate, water–surface hydrogen bonds can more easily

break, thus allowing water molecules to move away from the surface.

Because the simulation results are semi-quantitatively similar (e.g. the perturbation on water structure and dynamics due to the surface always extends for distances less than 1.0–1.5 nm), only access to detailed experimental data could permit a rigorous discrimination between the reliability of simulation predictions. To reproduce experimental observations, it is crucial to simulate the correct density of surface hydroxyl groups. Experimental contact angles could be used to fine-tune water–surface interaction parameters. To allow realistic dynamics of interfacial water, it appears important to include in the implemented models the possibility for the solid atoms to vibrate, thus exchanging momentum with interfacial water and promoting density fluctuations at the interface.

Acknowledgements

Financial support was provided, in part, by the Division of Chemical Sciences, Geosciences and Biosciences, Office of Basic Energy Sciences, US Department of Energy, by contract number DE-AC05-00OR22725 to the Oak Ridge National Laboratory (managed and operated by UT-Battelle, LLC), by the DoE EPSCoR, Office of Basic Energy Sciences, US Department of Energy, by contract number DE-SC0001902 to The University of Oklahoma and by the US National Science Foundation, by contract number CBET-0853657 to The University of Oklahoma. Generous allocations of computing time were provided by the OU Supercomputing Center for Education and Research (OSCER) at the University of Oklahoma and by the National Energy Research Scientific Computing Center (NERSC) at Lawrence Berkeley National Laboratory.

References

[1] S.R. Quake and A. Scherer, *From micro- to nanofabrication with soft materials*, Science American Association for the Advancement of Science 290 (2000), pp. 1536–1540.

[2] N.A. Mortensen, S.S. Xiao, and J. Pedersen, *Liquid-infiltrated photonic crystals: Enhanced light-matter interactions for lab-on-a-chip applications*, Microfluid. Nanofluid. 4 (2008), pp. 117–127.

[3] F. Fornasiero, H.G. Park, J.K. Holt, M. Stadermann, C.P. Grigoropoulos, A. Noy, and O. Bakajin, *Ion exclusion by sub-2-nm carbon nanotube pores*, Proc. Natl Acad. Sci. USA 105 (2008), pp. 17250–17255.

[4] B. Corry, *Designing carbon nanotube membranes for efficient water desalination*, J. Phys. Chem. B 112 (2008), pp. 1427–1434.

[5] K. Leung, S.B. Rempe, and C.D. Lorenz, *Salt permeation and exclusion in hydroxylated and functionalized silica pores*, Phys. Rev. Lett. 96 (2006) 095504.

[6] D. Argyris, D.R. Cole, and A. Striolo, *Ion-specific effects under confinement: The role of interfacial water*, ACS Nano American Chemical Society 4 (2010), pp. 2035–2042.

[7] D.J. Donaldson and K.T. Valsaraj, *Adsorption and reaction of trace gas-phase organic compounds on atmospheric water film surfaces: A critical review*, Environ. Sci. Technol. 44 (2010), pp. 865–873.

[8] D.R. Cole, E. Mamontov, and G. Rother, *Structure and dynamics of fluids in microporous and mesoporous earth and engineered materials,* in *Neutron Applications in Earth, Energy and Environmental Sciences*, L. Liang, R. Rinaldi and H. Schober, eds., Springer, New York, 2009, pp. 547–570.

[9] E. Mamontov, D.J. Wesolowski, L. Vlcek, P.T. Cummings, J. Rosenqvist, W. Wang, and D.R. Cole, *Dynamics of hydration water on rutile studied by backscattering neutron spectroscopy and molecular dynamics simulation*, J. Phys. Chem. C 112 (2008), pp. 12334–12341.

[10] N. Malikova, A. Cadène, V. Marry, E. Dubois, and P. Turq, *Diffusion of water in clays on the microscopic scale: Modeling and experiment*, J. Phys. Chem. B 110 (2006), pp. 3206–3214.

[11] A.L. Barnette, D.B. Asay, and S.H. Kim, *Average molecular orientations in the adsorbed water layers on silicon oxide in ambient conditions*, Phys. Chem. Chem. Phys. 10 (2008), pp. 4981–4986.

[12] Z. Zhang, P. Fenter, L. Cheng, N.C. Sturchio, M.J. Bedzyk, M. Predota, A. Bandura, J.D. Kubicki, S.N. Lvov, P.T. Cummings, A.A. Chialvo, M.K. Ridley, P. Benezeth, L. Anovitz, D.A. Palmer, M.L. Machesky, and D.J. Wesolowski, *Ion adsorption at the rutile-water interface: Linking molecular and macroscopic properties*, Langmuir 20 (2004), pp. 4954–4969.

[13] E.E. Fenn, D.B. Wong, and M.D. Fayer, *Water dynamics at neutral and ionic interfaces*, Proc. Natl Acad. Sci. USA 106 (2009), pp. 15243–15248.

[14] A. Striolo, A.A. Chialvo, P.T. Cummings, and K.E. Gubbins, *Water adsorption in carbon-slit nanopores*, Langmuir 19 (2003), pp. 8583–8591.

[15] A. Striolo, K.E. Gubbins, M.S. Gruszkiewicz, D.R. Cole, J.M. Simonson, and A.A. Chialvo, *Effect of temperature on the adsorption of water in porous carbons*, Langmuir 21 (2005), pp. 9457–9467.

[16] J.W. Wang, A.G. Kalinichev, and R.J. Kirkpatrick, *Effects of substrate structure and composition on the structure, dynamics, and energetics of water at mineral surfaces: A molecular dynamics modeling study*, Geochim. Cosmochim. Acta 70 (2006), pp. 562–582.

[17] E.M.L. Pedro, M. Vladimir, T. Mouhsine, D. Eugene, and D.M. Alexander, *Development of an empirical force field for silica. Application to the quartz − water interface*, J. Phys. Chem. B 110 (2006), pp. 2782–2792.

[18] G. Nagy, M.C. Gordillo, E. Guàrdia, and J. Martí, *Liquid water confined in carbon nanochannels at high temperatures*, J. Phys. Chem. B 111 (2007), pp. 12524–12530.

[19] N. Giovambattista, P.G. Debenedetti, and P.J. Rossky, *Hydration behavior under confinement by nanoscale surfaces with patterned hydrophobicity and hydrophilicity*, J. Phys. Chem. C 111 (2007), pp. 1323–1332.

[20] K. Shirono and H. Daiguji, *Molecular simulation of the phase behavior of water confined in silica nanopores*, J. Phys. Chem. C 111 (2007), pp. 7938–7946.

[21] S. Kerisit, C. Liu, and E.S. Ilton, *Molecular dynamics simulations of the orthoclase (001)- and (010)-water interfaces*, Geochim. Cosmochim. Acta 72 (2008), pp. 1481–1497.

[22] M.C.F. Wander and A.E. Clark, *Structural and dielectric properties of quartz–water interfaces*, J. Phys. Chem. C 112 (2008), pp. 19986–19994.

[23] M.C. Gordillo and J. Martí, *Molecular dynamics description of a layer of water molecules on a hydrophobic surface*, J. Chem. Phys., American Institute of Physics 117 (2002), p. 3425.

[24] A. Striolo, *The mechanism of water diffusion in narrow carbon nanotubes*, Nano Lett. 6 (2006), pp. 633–639.

[25] D. Argyris, N.R. Tummala, A. Striolo, and D.R. Cole, *Molecular structure and dynamics in thin water films at the silica and graphite surfaces*, J. Phys. Chem. C 112 (2008), pp. 13587–13599.

[26] D. Argyris, D.R. Cole, and A. Striolo, *Dynamic behavior of interfacial water at the silica surface*, J. Phys. Chem. C 113 (2009), pp. 19591–19600.

[27] D. Argyris, D.R. Cole, and A. Striolo, *Hydration structure on crystalline silica substrates*, Langmuir 25 (2009), pp. 8025–8035.

[28] C. Santiago Romero-Vargas, G. Nicolaás, A.A. Ilhan, and G.D. Pablo, *Evolution from surface-influenced to bulk-like dynamics in nanoscopically confined water*, J. Phys. Chem. B 113 (2009), pp. 7973–7976.

[29] J. Puibasset and R.J.M. Pellenq, *Grand canonical Monte Carlo simulation study of water structure on hydrophilic mesoporous and*

plane silica substrates, J. Chem. Phys. American Institute of Physics 119 (2003), p. 9226.
[30] S.R.V. Castrillon, N. Giovambattista, I.A. Aksay, and P.G. Debenedetti, *Effect of surface polarity on the structure and dynamics of water in nanoscale confinement*, J. Phys. Chem. B 113 (2009), pp. 1438–1446.
[31] S.H. Lee and P.J. Rossky, *A comparison of the structure and dynamics of liquid water at hydrophobic and hydrophilic surfaces: A molecular dynamics simulation study*, J. Chem. Phys. 100 (1994), pp. 3334–3345.
[32] A. Bródka and T.W. Zerda, *Properties of liquid acetone in silica pores: Molecular dynamics simulation*, J. Chem. Phys. 104 (1996), pp. 6319–6326.
[33] R.T. Cygan, J.J. Liang, and A.G. Kalinichev, *Molecular models of hydroxide, oxyhydroxide, and clay phases and the development of a general force field*, J. Phys. Chem. B 108 (2004), pp. 1255–1266.
[34] G.-M. Rignanese, J.-C. Charlier, and X. Gonze, *First-principles molecular-dynamics investigation of the hydration mechanisms of the (0001)[small alpha]-quartz surface*, Phys. Chem. Chem. Phys. 6 (2004), pp. 1920–1925.
[35] S. Nangia and B.J. Garrison, *Reaction rates and dissolution mechanisms of quartz as a function of pH*, J. Phys. Chem. A American Chemical Society 112 (2008), pp. 2027–2033.
[36] D. Ceresoli, M. Bernasconi, S. Iarlori, M. Parrinello, and E. Tosatti, *Two-membered silicon rings on the dehydroxylated surface of silica*, Phys. Rev. Lett. American Physical Society 84 (2000), p. 3887.
[37] P. Masini and M. Bernasconi, Ab initio *simulations of hydroxylation and dehydroxylation reactions at surfaces. Amorphous silica and brucite*, J. Phys. Condensed Matter 14 (2002), pp. 4133–4144.
[38] M.P. Allen and D.J. Tildesley, *Computer Simulation of Liquids*, Oxford University Press, Oxford, 2004.
[39] E. Lindahl, B. Hess, and D. van der Spoel, GROMACS 3.0: A package for molecular simulation and trajectory analysis, J. Mol. Model. 7 (2001), p. 306.
[40] B. Hess, C. Kutzner, D. van der Spoel, and E. Lindahl, GROMACS 4: Algorithms for highly efficient, load-balanced and scalable molecular simulation, J. Chem. Theory Comput. 4 (2008), p. 435.
[41] H.J.C. Berendsen, D. van der Spoel, and R. van Drunen, GROMACS: A message-passing parallel molecular dynamics implementation, Comput. Phys. Commun. 91 (1995), p. 43.
[42] D. van der Spoel, E. Lindahl, B. Hess, G. Groenhof, A.E. Mak, and H.J.C. Berendsen, GROMACS: Fast, flexible, and free, J. Comput. Chem. 26 (2005), pp. 1701–1708.
[43] J.P. Ryckaert, G. Ciccotti, and H.J.C. Berendsen, *Numerical-integration of Cartesian equations of motion of a system with constraints – Molecular-dynamics of n-alkanes*, J. Comput. Phys. 23 (1977), pp. 327–341.
[44] H.J.C. Berendsen, J.R. Grigera, and T.P. Straatsma, *The missing term in effective pair potentials*, J. Phys. Chem. 91 (1987), pp. 6269–6271.
[45] U. Essmann, L. Perera, M.L. Berkowitz, T. Darden, H. Lee, and L.G. Pedersen, *A smooth particle mesh Ewald method*, J. Chem. Phys., American Institute of Physics 103 (1995), p. 8577.
[46] H.J.C. Berendsen, J.P.M. Postma, E.F. van Gunsteren, and J. Hermans, *Intermolecular Forces*, D. Reidel, Dordrecht, 1981.
[47] H. Margenau and N.R. Kestner, *Theory of Intermolecular Forces*, Pergamon Press, Oxford, 1969.
[48] M.A. Ricci, F. Bruni, P. Gallo, M. Rovere, and A.K. Soper, *Water in confined geometries: Experiments and simulations*, J. Phys. Condensed Matter 12 (2000), pp. A345–A350.
[49] P. Gallo, M.A. Ricci, and M. Rovere, *Layer analysis of the structure of water confined in vycor glass*, J. Chem. Phys. (2002), 116 pp. 342–346.
[50] L.G. MacDowell, M. Müller, and K. Binder, *How do droplets on a surface depend on the system size?* Colloids Surfaces A: Phys. Eng. Asp. 50 (2002), p. 277.
[51] T. Werder, J.H. Walther, R.L. Jaffe, T. Halicioglu, and P. Koumoutsakos, *On the water–carbon interaction for use in molecular dynamics simulations of graphite and carbon nanotubes (vol. 107B, p. 1349, 2003)*, J. Phys. Chem. B 112 (2008), p. 14090.
[52] T. Ingebrigtsen and S. Toxvaerd, *Contact angles of Lennard-Jones liquids and droplets on planar surfaces*, J. Phys. Chem. C 111 (2007), pp. 8518–8523.
[53] J. Marti, G. Nagy, E. Guardia, and M.C. Gordillo, *Molecular dynamics simulation of liquid water confined inside graphite channels: Dielectric and dynamical properties*, J. Phys. Chem. B 110 (2006), pp. 23987–23994.
[54] E. Mamontov, L. Vlcek, D.J. Wesolowski, P.T. Cummings, W. Wang, L.M. Anovitz, J. Rosenqvist, C.M. Brown, and V.G. Sakai, *Dynamics and structure of hydration water on rutile and cassiterite nanopowders studied by quasielastic neutron scattering and molecular dynamics simulations*, J. Phys. Chem. C 111 (2007), pp. 4328–4341.
[55] J.W. Wang, A.G. Kalinichev, and R.J. Kirkpatrick, *Asymmetric hydrogen bonding and orientational ordering of water at hydrophobic and hydrophilic surfaces: A comparison of water/vapor, water/talc, and water/mica interfaces*, J. Phys. Chem. C 113 (2009), pp. 11077–11085.
[56] R. Godawat, S.N. Jamadagni, and S. Garde, *Characterizing hydrophobicity of interfaces by using cavity formation, solute binding, and water correlations,* Proc. Natl Acad. Sci. USA 106 (2009), pp. 15119–15124.
[57] R.S. Voronov, D.V. Papavassiliou, and L.L. Lee, *Review of fluid slip over superhydrophobic surfaces and its dependence on the contact angle*, Ind. Eng. Chem. Res. 47 (2008), pp. 2455–2477.
[58] J. Marti, *Analysis of the hydrogen bonding and vibrational spectra of supercritical model water by molecular dynamics simulations*, J. Chem. Phys. 110 (1999), pp. 6876–6886.
[59] Y.S. Djikaev and E. Ruckenstein, *A probabilistic approach to the effect of hydrogen bonding on the hydrophobic attraction*, J. Chem. Phys. 130 (2009), 124713.
[60] A. Chandra, *Effects of ion atmosphere on hydrogen-bond dynamics in aqueous electrolyte solutions*, Phys. Rev. Lett. 85 (2000), pp. 768–771.

Appendix A: SPC vs. SPC/E water

In Figure A1, we show the water oxygen (a) and hydrogen (b) atomic density profiles for both SPC/E and SPC models of water simulated on LD surfaces. In Figure A2, we present simulation results obtained on HD surfaces. All simulations are conducted at 300 K. Although small differences can be observed, especially, when the peak intensities obtained for SPC or SPC/E models of water are compared on the same surface, our results show that the peak positions do not depend on the model implemented to describe water. We conclude that implementing either SPC/E or SPC model to describe the structural properties of interfacial water yields comparable results.

Appendix B: Surface density distributions on HD silica surfaces

In Figure A3, we report the surface distributions of water oxygen atoms belonging to HAO-1 (a) and HAO-2 (b) layers on the HD-PER surface. Peak positions are reported in Table 4. The results in Figure A3(a) indicate that oxygen atoms belonging to the HAO-1 layer concentrate in well structured regularly distributed narrow areas. These areas are found at vertices 1, 3 and 5 of the hexagons formed by surface silicon atoms (see Figure A4). On the second layer (HAO-2), as shown in Figure A3(b), oxygen atoms of interfacial water accumulate at vertices 2, 4 and 6 of the silicon hexagons (Figure A4), suggesting that the surface alters

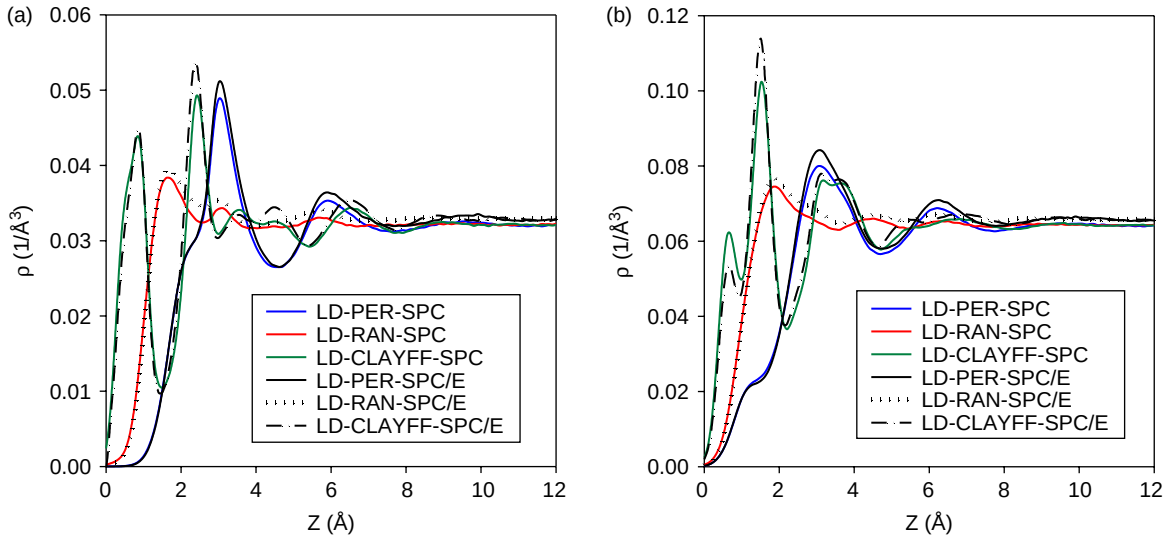

Figure A1. Oxygen (a) and hydrogen (b) atomic density profiles for SPC/E and SPC water as a function of the distance z from the LD surfaces at 300 K. The reference $z = 0$ is the plane of non-bridging oxygen atoms of the bottom slab (see Figure 3).

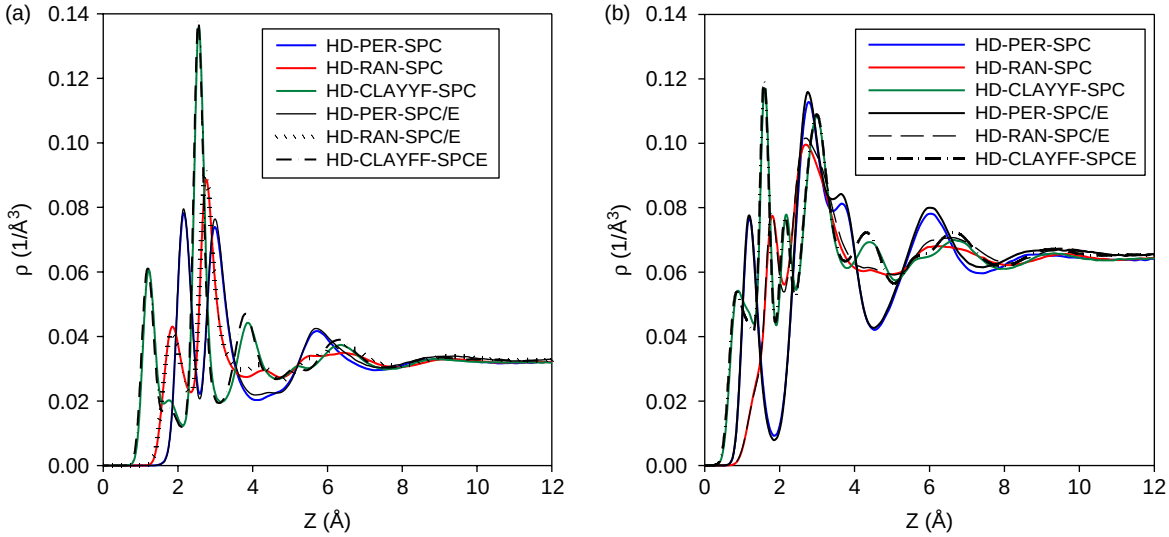

Figure A2. Oxygen (a) and hydrogen (b) atomic density profiles for SPC/E and SPC water as a function of the distance z from the HD surfaces at 300 K. The reference $z = 0$ is the plane of non-bridging oxygen atoms of the bottom slab (see Figure 3).

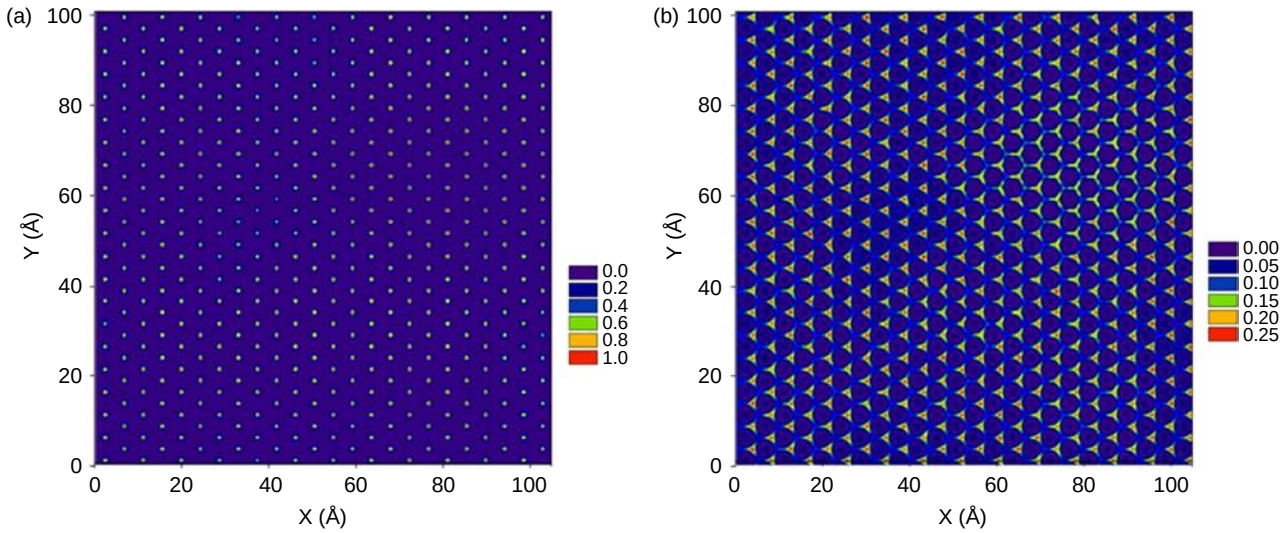

Figure A3. Surface density distributions for oxygen atoms of interfacial water near HD-PER surfaces. Panels (a) and (b) represent results for HAO-1 and HAO-2 layers, respectively. See Table 4 for peak positions. Surface densities are expressed as number of atoms per $Å^3$.

the structure of interfacial water, compared to that observed in the bulk, for distances larger than the LD surface does (see Section 3.3) because of water–water preferable interactions. This effect is enabled by the high density of rigid hydroxyl groups on the HD-PER surface.

The surface distribution of hydrogen atoms belonging to the HAH-1 layer (Figure A5(a)) is analogous to the distribution of oxygen atoms in the HAO-1 layer. As observed in the case of LD surfaces, this analogous density distribution, coupled to the fact that the distance between HAH-1 and HAO-1 layers is 1 Å, implies that those water molecules whose oxygen atoms belong to layer HAO-1 assume hydrogen-down orientation. Hydrogen atoms belonging to the HAH-2 layer (Figure A5(b)) show a multi-modal distribution, although with a significant amount of order. The hydrogen atoms in this layer belong to water molecules whose oxygen atoms are in either layer HAO-1 or in layer HAO-2.

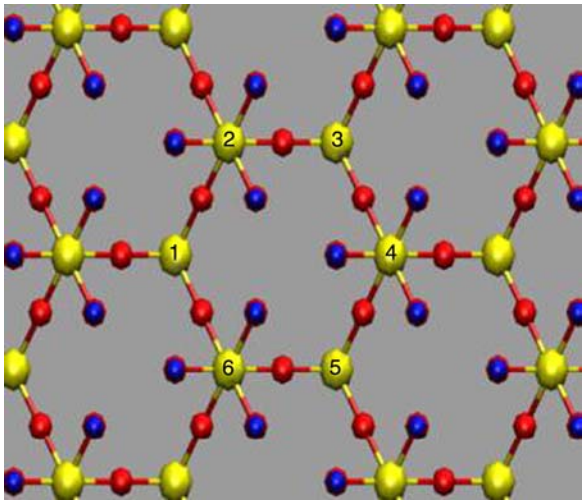

Figure A4. Hexagon formed by silicon atoms on the HD-surface. The numbers identify six vertices of the hexagon. Only surface atoms are shown for clarity.

In Figure A6(a) and (b), we provide the surface distributions of oxygen atoms belonging to layer HBO-1 and HBO-2 on the HD-RANDOM surface, respectively. The density distribution on the HBO-1 layer resembles that found on the HD-PER surface (see Figure A3(a)), although a number of imperfections emerge in the hexagonal distribution of oxygen atoms, reflecting the random orientation of the surface hydroxyl groups. The surface distribution of oxygen atoms in layer HBO-2 (Figure A6(b)) indicates that the water molecules are rather disordered along the *X* and *Y* directions. In Figure A6(c) and (d), we show the surface distributions of hydrogen atoms belonging to HBH-1 and HBH-2 layers, respectively. Because of the random orientation of the surface hydroxyl groups, the density distribution of hydrogen atom in layer HBH-1 (Figure A6(c)) resembles that in layer HAH-1 (Figure A5(a)), but the locations with high atomic density have variable intensity. The effect becomes more pronounced on the second layer (compare Figure A6(d) to Figure A5(b)).

In Figure A7(a), we show the surface distribution of surface hydrogen atoms of the HD-CLAYFF surface. Because the hydrogen atoms on the HD-CLAYFF surface rotate on a plane perpendicular to the Si-O vector (Figure 2(b)), the movement of three hydrogen atoms belonging to one silanol group yields the arcs highlighted by the green circle in Figure A7(a). However, the surface hydrogen atoms do not regularly distribute along these arcs because of preferential interactions with interfacial water. The surface distributions of oxygen atoms belonging to HCO-1 and HCO-2 layers (Figure A7(b) and (c)) are the same as those in layers HBO-1 and HBO-2, respectively. It is instructive to note that in correspondence to layer HCH-1 (Figure A7(d)), the hydrogen atoms assume a distribution very similar to that of oxygen atoms in layer HCO-1.

In Figure A8, we show the surface distributions of oxygen atoms belonging to HDO-1 (a) and HDO-2 (b) layers on the HD-CLAYFF-RIGID surface. The surface distributions of oxygen atoms of HDO-1 and HDO-2 layers are the same as those found on layers HCO-1 and HCO-2, respectively. It appears that on the HD surfaces modelled with the CLAYFF force field, allowing for

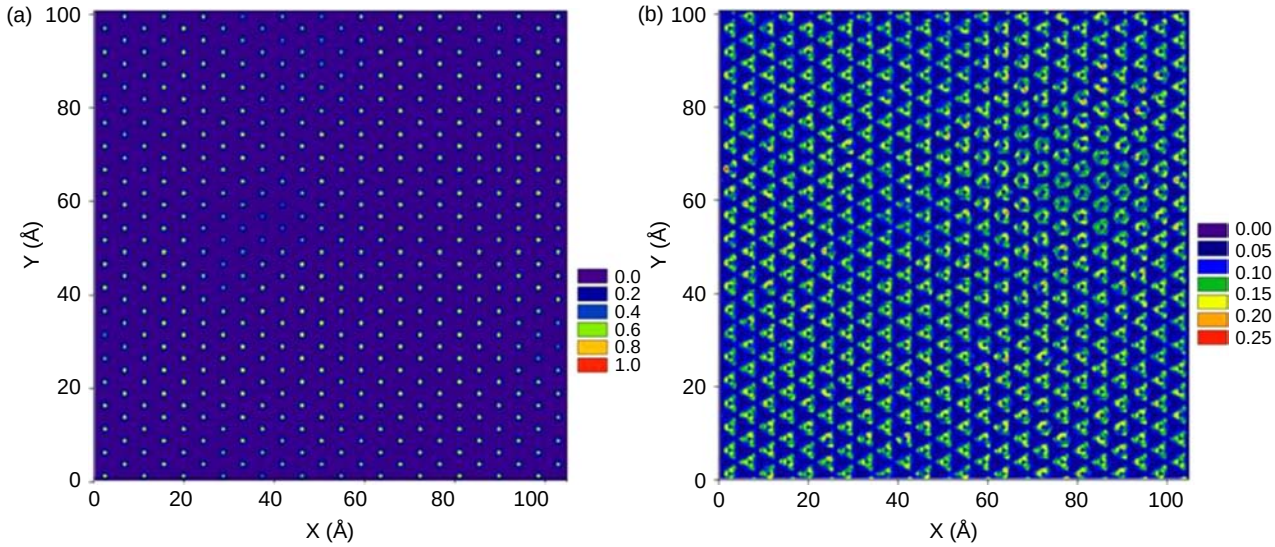

Figure A5. Surface density distributions for hydrogen atoms of interfacial water on HD-PER surfaces. Panels (a) and (b) represent results for HAH-1 and HAH-2 layers, respectively. See Table 4 for peak position. Surface densities are expressed as number of atoms per $Å^3$.

the rotation of surface hydrogen atoms has little effect on the in-plane atomic density distributions, which is contrary to what was observed on the LD surfaces (see Section 3.4). This different result is due to the differences of the orbit of surface hydrogen atoms rotation on LD and HD surfaces (see Figure 2).

It appears that the structure of water on the silica surfaces with high density of hydroxyl groups is less sensitive to the details of the force field implemented to describe the solid substrate, in qualitative agreement with contact angle observations discussed in Section 3.1. However, we point out that the density profiles on the direction perpendicular to the surface (Section 3.3), as well as the dynamic properties of interfacial water (Section 3.5), strongly depend on the details used to describe the solid substrates.

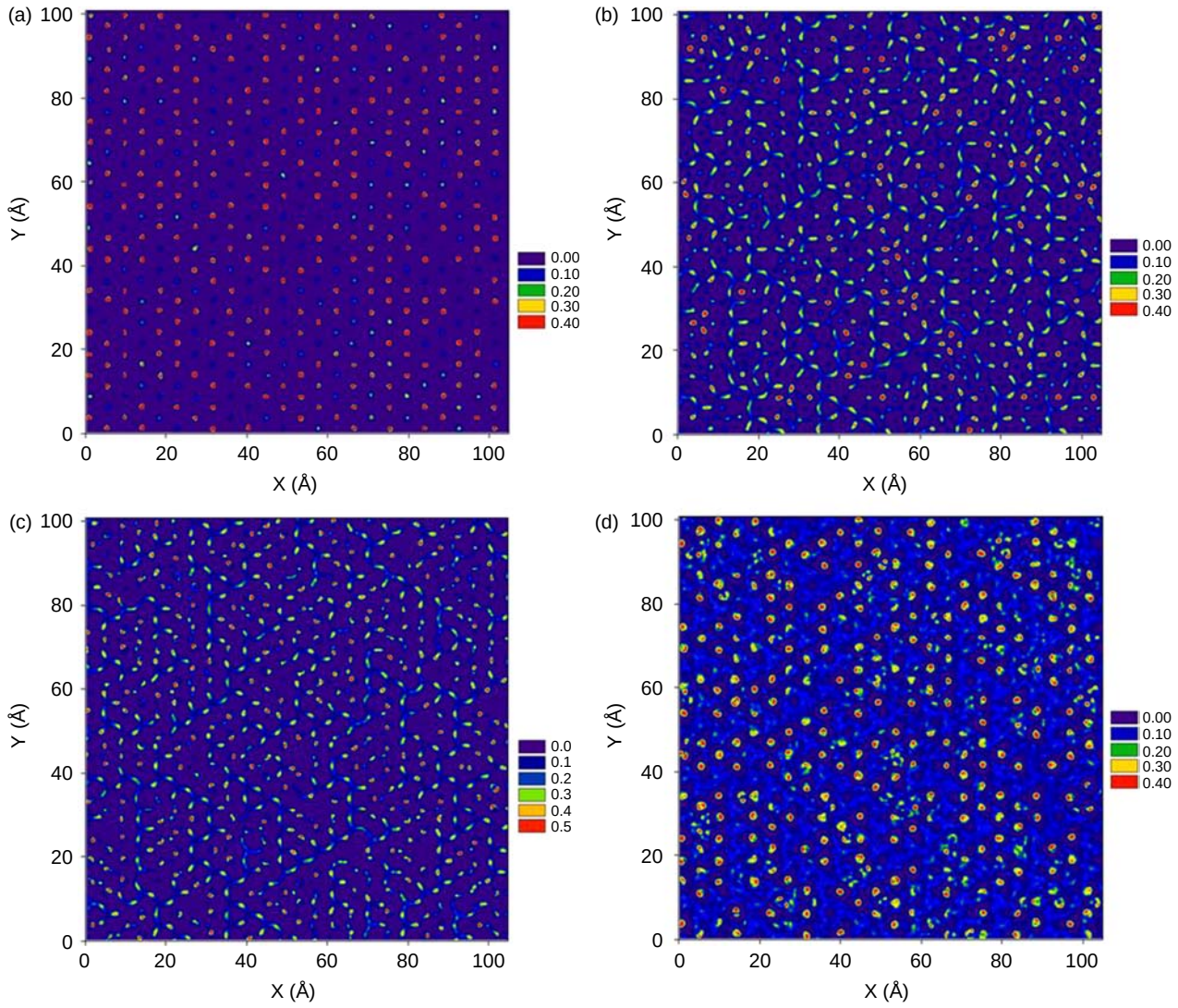

Figure A6. Surface density distributions of oxygen atoms in layers HBO-1 (a) and HBO-2 (b), and of hydrogen atoms in layers HBH-1 (c) and HBH-2 (d) on the HD-RANDOM surface. See Table 4 for details on peaks position. Surface densities are expressed as number of atoms per $Å^3$.

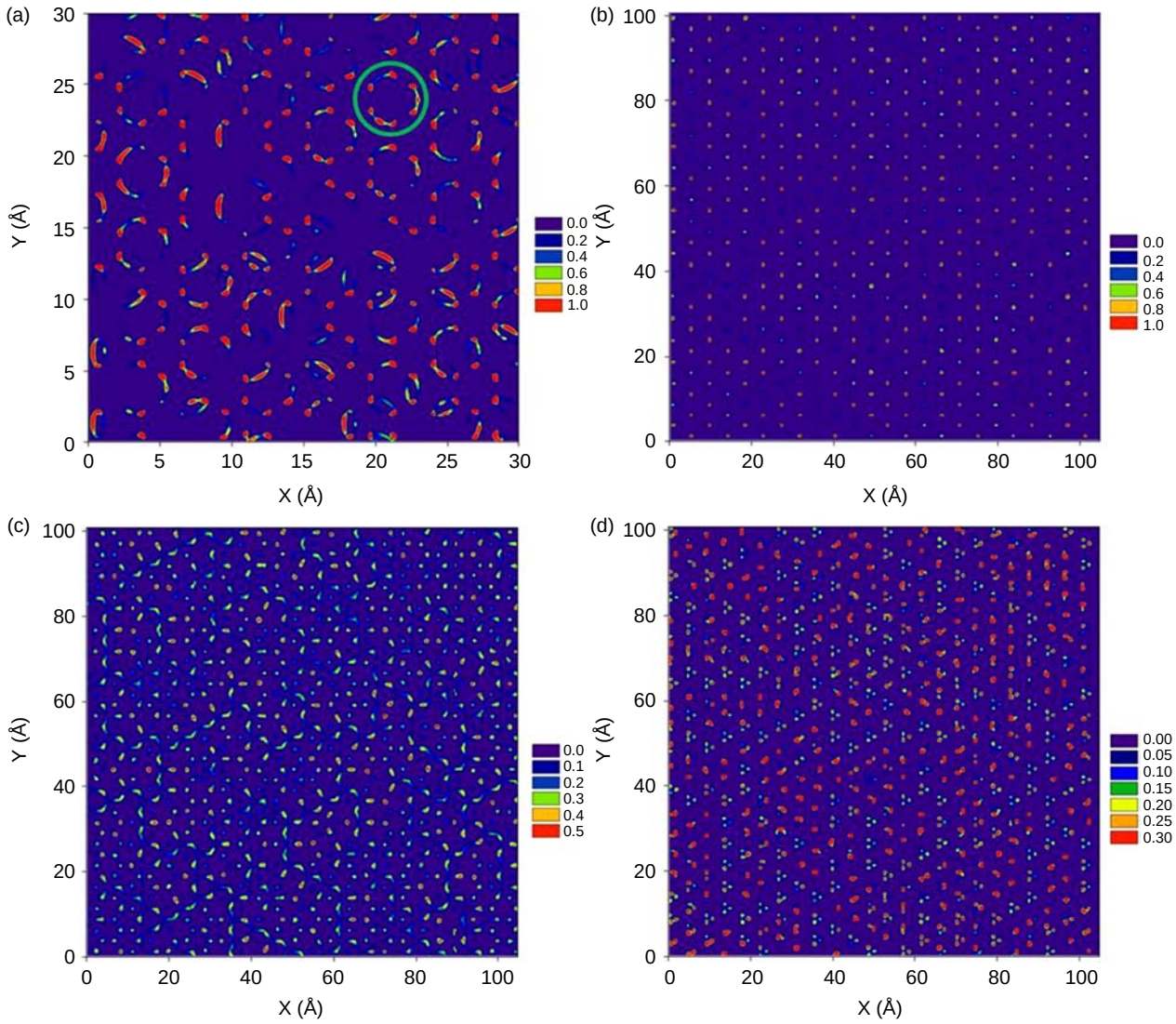

Figure A7. Surface density distributions of surface hydrogen atoms (a), water oxygen atoms belonging to HCO-1 (b) and HCO-2 (c), and water hydrogen atoms belonging to layer HCH-1 (d) on the HD-CLAYFF surface. See Table 4 for details on peaks position. Note that, for clarity, an enlargement of the (*X*,*Y*) plane, rather than the entire surface, is provided in panel (a). Surface densities are expressed as number of atoms per $Å^3$.

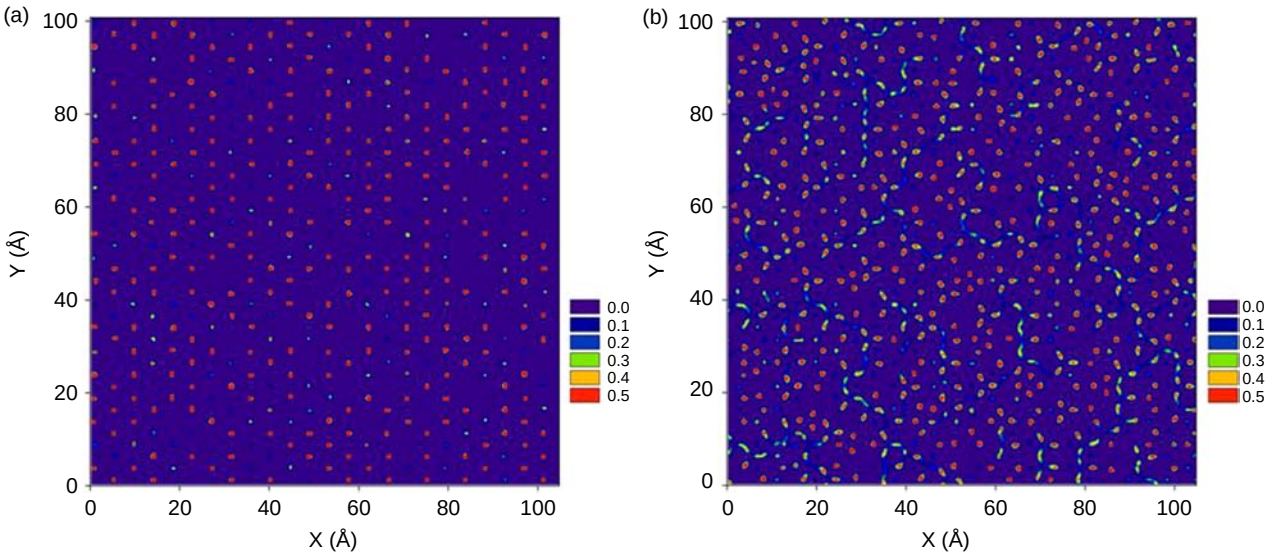

Figure A8. Surface density distributions of oxygen atoms belonging to HDO-1 (a) and HDO-2 (b) layers on HD-CLAYFF-RIGID surface. See Table 4 for details on peak position. Surface densities distributions are expressed in number of atoms per $Å^3$.